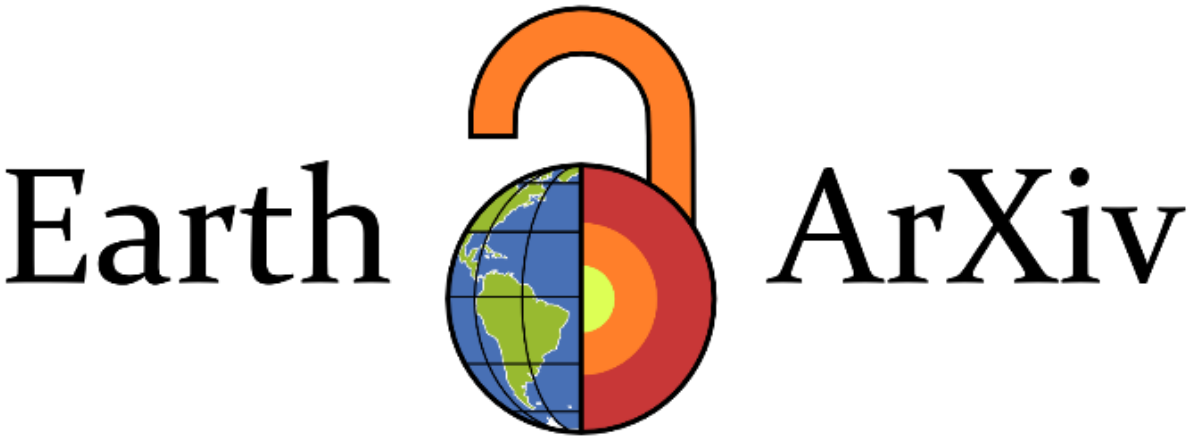

Insights from the Unseen - Occlusion in Forest Laser Scanning

Daniel Kükenbrink[a,1,*], Matthias Gassilloud[b,1], Benjamin Brede[c], Aline Bornand[n], Kim Calders[j], Wout Cherlet[j], Markus P Eichhorn[d,e], Julian Frey[i], Charis Moana Gretler[a], Bernhard Höfle[h,g], Teja Kattenborn[b], Lennart Klinger[m], Martin Mokroš[l], Timo P Pitkänen[f], Ninni Saarinen[k], Louise Terryn[j], Hannah Weiser[h,g], Anna Göritz[b]

[a]*Landchange Science, Swiss Federal Institute WSL, Zürcherstrasse 111, Birmensdorf, CH-8903, Switzerland*
[b]*Chair of Sensor-based Geoinformatics (geosense), University of Freiburg, Tennenbacherstr. 4, D-79106, Freiburg, Germany*
[c]*GFZ Helmholtz Centre for Geosciences, Telegrafenberg, Potsdam, 14473, Germany*
[d]*School of Biological, Earth & Environmental Sciences,University College Cork, Distillery Fields, North Mall, Cork, T23 N73K, Ireland*
[e]*Sustainability Institute, University College Cork, Lee Rd, Sunday's Well, Cork, T23 XE10, Ireland*
[f]*Natural Resources Institute Finland (LUKE), Latokartanonkaari 9, Helsinki, FI-00790, Finland*
[g]*3DGeo Research Group, Institute of Geography, Heidelberg University, Im Neuenheimer Feld 368, Heidelberg, 69120, Germany*
[h]*Interdisciplinary Center for Scientific Computing (IWR), Heidelberg University, Im Neuenheimer Feld 205, Heidelberg, 69120, Germany*
[i]*Forest Growth and Dendroecology, University of Freiburg, Tennenbacherstr. 4, Freiburg, 79106, Germany*
[j]*Q-ForestLab, Department of Environment, Faculty of Bioscience Engineering, Ghent University, Belgium, Campus Coupure, Coupure links 653, Ghent, 9000, Belgium*
[k]*School of Forest Sciences, University of Eastern Finland, P.O. Box 111, Joensuu, FI-80101, Finland*
[l]*Department of Geography, University College London, Gower Street, London, WC1E6BT, UK*
[m]*Laboratory of Geo-Information Science and Remote Sensing, Wageningen University, Droevendaalsesteeg 3, Gaia, building number 101, Wageningen, 6708 PB, the Netherlands*
[n]*Forest Resources and Management, Swiss Federal Institute WSL, Zürcherstrasse 111, Birmensdorf, CH-8903, Switzerland*

*Corresponding author: daniel.kuekenbrink@wsl.ch
[1]These authors contributed equally to this work

Abstract

Laser scanning is a powerful tool for assessing the structural complexity of forests and its role in ecosystem processes and functioning. However, laser scanning acquisitions are inherently affected by occlusion (where objects block laser pulses), resulting in unobserved volumes within the 3D representation of the forest. Although occlusion is a well-known and frequently discussed challenge for estimating forest structural information from laser scanning data, it is rarely quantified.

Here, we offer a perspective on occlusion in forest laser scanning, aimed at researchers across the forest remote sensing community, ranging from point cloud specialists to ecologists relying on laser scanning derived structural products. We define and distinguish the principal types of occlusion, and examine their primary causes across multiple platforms (terrestrial [TLS], mobile [MLS], UAV-borne [ULS], and airborne [ALS] laser scanning platforms). We discuss platform-specific challenges and practical strategies to minimise occlusion across diverse forest types and acquisition scenarios. We further synthesise available tools for occlusion detection and mapping, and highlight key research opportunities, spanning uncertainty quantification, point cloud completion, virtual laser scanning, and intelligent autonomous laser scanning acquisition design. By framing occlusion as a mappable and actionable property of laser scanning data, this perspective aims to promote more rigorous assessments of point cloud suitability and inspire methodological advances

in forest structural assessment.

Keywords: LiDAR, occlusion, point cloud quality, forest structure, raytracing, volume exploration, ULS, MLS, TLS

1. Introduction

Forest structure plays a vital role in ecological processes and ecosystem functioning. It regulates how solar radiation is absorbed, transmitted, and reflected (Kükenbrink et al., 2021), influencing processes related to energy and matter fluxes (Damm et al., 2020; Kesselring et al., 2024), and microclimate (Zellweger et al., 2020). The structure of forests determines habitat availability and heterogeneity, making it a key control for biodiversity (Helbach et al., 2022; Knuff et al., 2020; Heidrich et al., 2020), and it is closely linked to aboveground biomass and carbon storage (Lefsky et al., 2002). Consequently, assessing forest structure is essential for understanding forest dynamics and functioning in the face of climate change and the biodiversity crisis (Ehbrecht et al., 2021; Pan et al., 2013; Pörtner et al., 2021).

Laser scanning (also called Light detection and ranging (LiDAR)) technologies have become an important tool for quantifying forest structure at a high level of detail and accuracy. Laser scanning, which collects spatial information from the reflections of emitted laser beams, can capture the 3D distribution of vegetation components, enabling the assessment of tree crown dimensions, foliage distribution, and 3D complexity (Calders et al., 2020; Ehbrecht et al., 2026; Frey et al., 2025; Liang et al., 2022). By provid-

ing such detailed 3D structural information, laser scanning plays a crucial role in addressing pressing research questions related to biodiversity (Toivonen et al., 2023), habitat heterogeneity (Moudrý et al., 2023; Helbach et al., 2022), biomass distribution (Seidel et al., 2011), disturbance impacts (Barrere et al., 2024; Jactel et al., 2017) and facilitates modelling of forest responses to environmental change (Calders et al., 2025).

Despite the widespread use of laser scanning for forest structural assessments, the acquired point clouds are rarely critically evaluated regarding their suitability to answer the posed research questions. It is often assumed that acquired point clouds adequately represent the targeted forest structural parameters (e.g. that the laser scanning acquisition captures the full vertical foliage distribution) without quantitative verification. Where accurate reference measurements exist for parameters such as tree height, diameter at breast height (DBH), or tree position, point cloud quality can be assessed through the accuracy of derived metrics. However, for many ecologically important structural parameters – including canopy layering, plant area density (PAD), leaf area index (LAI), and structural complexity – accurate reference measurements are inherently difficult to obtain, making validation and calibration challenging. In such cases, unexamined assumption of representativeness – here understood as the degree to which a point cloud captures the actual 3D structural composition of the forest, including both vegetation and gaps – can easily lead to biased conclusions and limit the transferability of methods across forest types and acquisition scenarios.

Assessing the quality of a point cloud in terms of its suitability is not a trivial task, and so far no robust and generic method for such an assessment exists. Most often, simple point cloud metrics such as point density or minimum distance between neighbouring points are used to indicate the completeness or quality of a point cloud (e.g., Wilkes et al., 2017; Calders et al., 2020). Point density metrics offer only a limited perspective on a point cloud's ability to capture structural complexity though, indicating point spacing but not the actual forest volume represented. Recent studies have shown that point density alone is a poor predictor of accuracy in derived forest parameters (e.g. above ground biomass, basal area, various height metrics, stem density) (Torralba et al., 2022) and that sample completeness and representativeness depend more strongly on scanning setup and viewpoint geometry (Abegg et al., 2017; Boucher et al., 2021; Nguyen et al., 2022).

Since forest volume comprises both vegetation and gaps, understanding point cloud completeness or representativeness requires analysing not just the captured vegetation, but also the spaces between objects. Gaps in the acquired forest point clouds are caused by either a) true empty space, b) missed objects, which lie between laser beams, or whose reflected energy falls below the detection threshold of the sensor, or c) occlusion, where an object obstructs further beam propagation. While the first two causes are primarily properties of the forest structure itself, the scan design, or the sensor characteristics, occlusion arises from the interaction between the scanning geometry and the scene being measured. Empirical assessments have shown

that occlusion can substantially limit the completeness and representativeness of laser scanning acquisitions, even with a very dense acquisition strategy (Abegg et al., 2017; Boucher et al., 2021). This raises the broader conceptual challenge of *how to know what we do not know* (Disney, 2021): quantifying not only the vegetation a point cloud captures, but also the volume it fails to observe. Occlusion can therefore substantially reduce the representativeness of the resulting point cloud, limiting the capacity to capture key forest structural parameters, including those relevant to the calibration and validation of spaceborne remote sensing products such as canopy height, PAD and LAI.

Only a few studies have explicitly addressed occlusion, primarily focusing on assessing point cloud coverage and completeness (e.g. Boucher et al., 2021; Brede et al., 2022; Gassilloud et al., 2025; Kükenbrink et al., 2017; Morsdorf et al., 2018), with a smaller body of work investigating the effect of occlusion on specific structural metrics (e.g. Ehbrecht et al., 2026; Nguyen et al., 2022; Schneider et al., 2019b; Yun et al., 2019). Most studies using laser scanning for forest attribute estimation address occlusion only implicitly, for instance, through regularised scan position distributions in terrestrial laser scanning (TLS) campaigns (e.g. Wilkes et al., 2017) or fixed overlaps between flight lines for unoccupied aerial vehicle laser scanning (ULS) acquisitions (e.g. Gassilloud et al., 2025), without accounting for variation in forest structure. The impact of occlusion on the estimation of forest structural metrics is rarely considered at all. There is therefore a critical gap in effective and scalable methods to map and account for occlusion across forest types,

scanning platforms, and acquisition scenarios. By systematically implementing occlusion mapping in forest structural assessments and accounting for its effects on derived metrics, the robustness of laser scanning–based analyses can be greatly enhanced. This, in turn, would substantially improve the ability to quantify structural changes from repeated acquisitions and strengthen forest monitoring capabilities.

Here we present a focused review and perspective on occlusion in forest laser scanning. Rather than a systematic review on forest LiDAR sensing, it is organised around a single premise: that occlusion, rather than being only a challenge to minimise, can be treated as a mappable and actionable property of laser scanning data, which opens up new pathways for forest LiDAR research and applications. We bring together the conceptual basis, causes, mitigation strategies, and available mapping tools for occlusion, and use them to develop this perspective. Specifically, this perspective aims to:

1. clarify the concept of occlusion and define its principle types across laser scanning platforms (TLS, mobile laser scanning (MLS), ULS, airborne laser scanning (ALS));
2. discuss the causes of occlusion and practical strategies to minimise its effects across diverse forest types and acquisition scenarios;
3. synthesise available methods and tools for occlusion mapping and discuss their applicability and limitations;
4. highlight key research opportunities that arise from explicitly incorporating occlusion into assessments of forest structure and derived bio-

physical products.

2. Defining occlusion: what is happening to laser pulses?

Laser scanning data of forests are typically obtained from ground-based, stationary (multi-station) TLS or MLS acquisitions or from aerial platforms, such as drones or air-planes (ULS, ALS). The different view-points and sensor characteristics can have various consequences and magnitudes regarding occlusion (see Section 3). Occlusion occurs when objects that could be detected by a laser beam are missed because the beam is blocked by intervening objects. This results in gaps within the point cloud, which are not truly empty but rather artefacts of the scanning process. Figure 1 schematically illustrates the interaction between laser pulses of a TLS acquisition and the causes for the different types of occlusion.

2.1. Types of occlusion and related pulse penetration metrics

Three fundamental types of occlusion can be distinguished based on their causes: absolute, geometric, and sub-footprint occlusion (Figure 1).

Absolute occlusion (pannels (b) and (c) in Figure 1) occurs when a laser pulse is entirely blocked or absorbed, making it impossible to overcome using any scanner technology or acquisition protocol. For example, the interiors of tree trunks cannot be captured by laser scanning. Also wavelength specific absorption can lead to absolute occlusion. For example, many TLS systems for forestry applications have wavelengths in a water absorption band of the

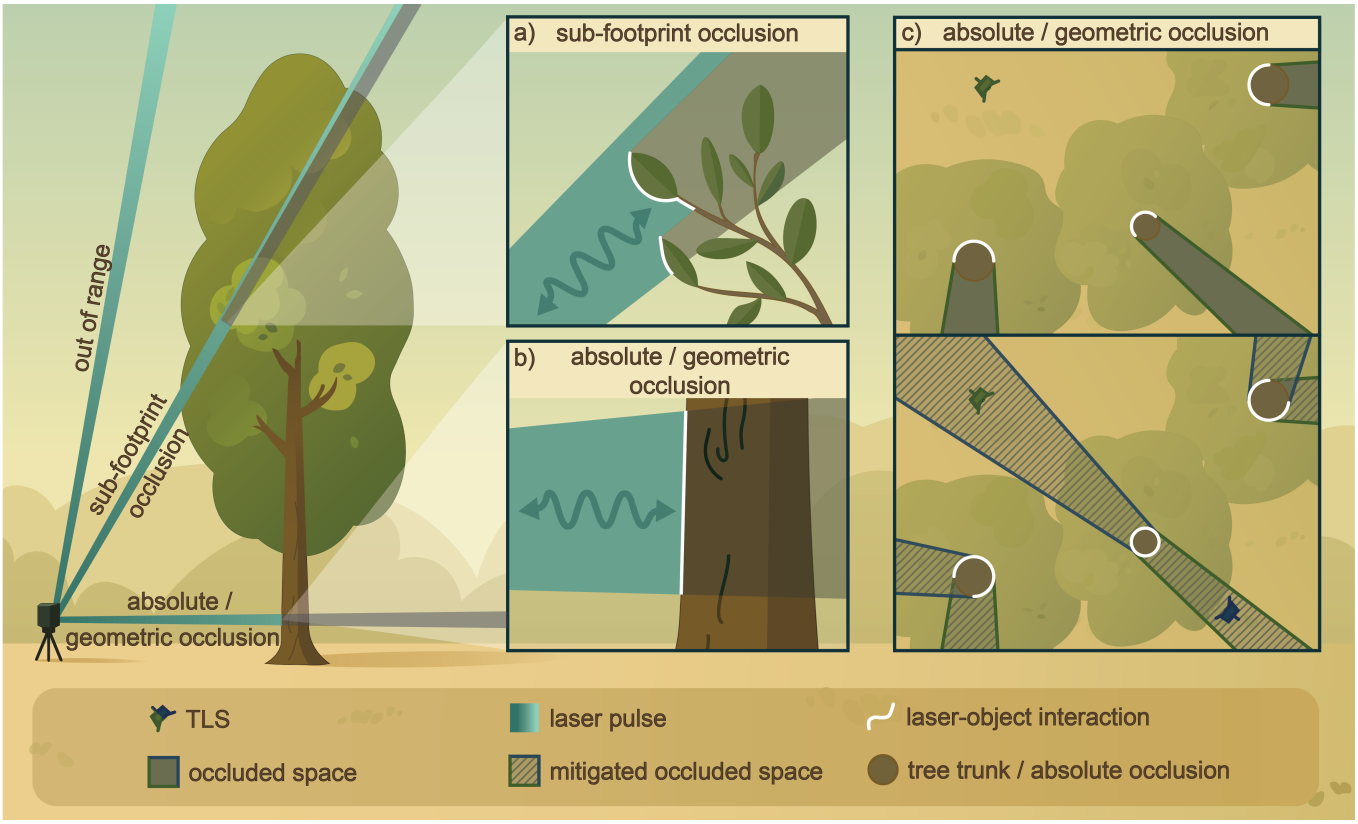

Figure 1: Definition of different occlusion types. Left part of the figure shows the three different occlusion types from a laser beam perspective. Note that the laser beam dimensions are exaggerated for visualization purposes. For the sub-footprint occlusion example (a) we assume complete reflection and absorption of the interacting part of the laser footprint with the leaf. Note that depending on the wavelength and pulse power, part of the laser pulse may also transmit through the leaf, potentially leading to a laser return behind the visualized leaves (similar to the blue part of the shown laser pulse that did not interact with the leaves). The right side of the figure (c) shows the difference between absolute and geometric occlusion from a single and multi-station TLS acquisition as shown from a top view perspective. Geometric occlusion found in the single station setup (top-right box) can be overcome by an additional scan station, hence these occluded areas were mitigated. The outline of the occluded area is coloured based on the colour of the TLS that cannot observe this area.

electromagnetic spectrum (e.g. at 1550 nm for Riegl VZ-400i). This can result in absolute or partial absorption of the laser pulses, depending on the object being scanned. Typically snow cover or water bodies can cause absolute absorption of the incoming laser pulses and consequently result in

occluded space. Therefore, it is always important to select an appropriate LiDAR device for the intended application.

Geometric occlusion occurs when objects are between the laser scanner and the target volume, but the occluding effect could be overcome if the target were observed from another viewing direction (area labeled as mitigated occluded space in Figure 1 in panel (c)). This type of occlusion is largely determined by the structural arrangement of the vegetation. An example would be the volume behind a trunk when observed from only one side with e.g. TLS. With an additional scan position, this volume could be observed, as shown in panel (c) of Figure 1.

Sub-footprint occlusion (panel (a) in Figure 1) involves beams that are not completely blocked but are partially absorbed or scattered, causing their returned energy to fall below the LiDAR's detection threshold. This occurs when laser pulses strike the edges of objects, which is particularly significant in forests where leaves present a fragmented set of surfaces. The extent of partial occlusion depends on the characteristics of both the laser scanner (e.g. laser pulse power, wavelength, beam divergence, detector sensitivity) and the material through which pulses are passing (e.g. reflectivity, degree of fragmentation). There is also the case when objects are out of range for the scanner. Here, similarly to partial occlusion, insufficient energy is returned to the detector. Since no objects are in between the potential target and the scanner, this scenario is not considered as occlusion.

Occlusion is closely related to a broader family of metrics describing how

laser pulses penetrate the canopy. Several of these — the gap fraction, the laser penetration rate, and their complement the canopy fractional cover — quantify the proportion of emitted pulses that traverse the canopy without interception along a given direction (e.g. Morsdorf et al., 2006; Hopkinson and Chasmer, 2009). For above-canopy acquisitions this is classically expressed as the ratio of ground to total returns, whereas for ground-based acquisitions the analogous quantity is the fraction of pulses passing unobstructed through the canopy (e.g. to open sky), typically resolved by zenith-angle ring (e.g. Danson et al., 2007). Others capture penetration in different ways: the canopy transmittance, for instance, is a physically defined radiometric quantity estimated from (full-waveform) returned energy rather than return counts, and can be derived per beam and mapped spatially (Milenković et al., 2017). Despite their differences, all of these metrics summarise penetration in aggregate; they do not, by themselves, distinguish space that was observed and found empty from space that was never sampled because intervening material blocked the beam. Occlusion mapping is in this sense complementary: rather than summarising penetration in aggregate, it spatially localises where the 3D scene remained unobserved. This is a prerequisite for attributing data gaps to true empty space versus blocked sampling (see Section 3.5).

2.2. From individual pulses to acquisitions

Since standard point cloud data formats, such as LAS or PLY, merely hold information about the captured laser returns, they do not directly in-

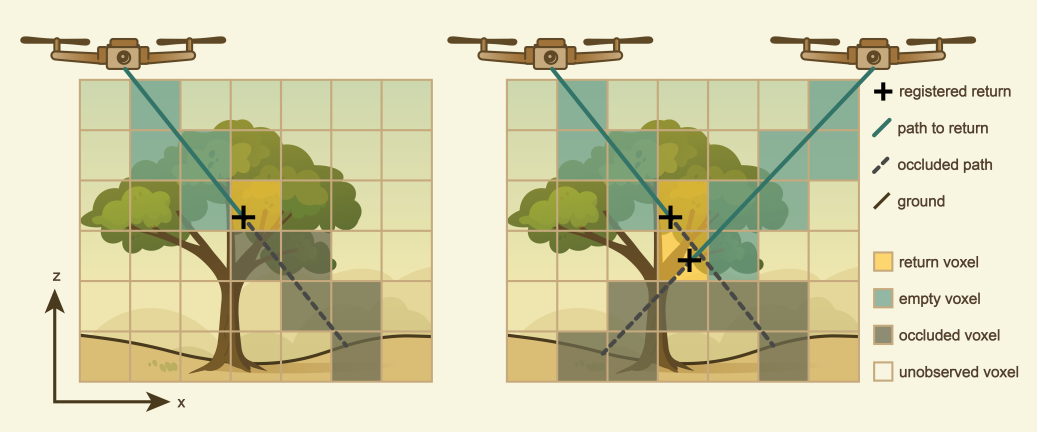

Figure 2: Schematic figure for a voxel traversal algorithm to map occlusion, indicating empty, return, occluded, and unobserved voxels. Left figure shows the voxel traversal and classification of a single pulse emitted from a single location. The right figure shows the same situation with two emitted pulses from two positions. By adding multiple pulses, voxels that have been occluded can be re-classified as observed.

form about occluded forest volumes in the acquisition. A relatively simple way to evaluate the scanned 3D space with respect to occlusion is to discretize the forest volume into a so-called voxel grid. A voxel is basically a 3D representation of a pixel with a pre-defined dimension. By employing a voxel traversal algorithm, such as the one introduced by Amanatides and Woo (1987), each laser pulse is traced through the voxel grid. Following the classification scheme proposed by Bienert et al. (2010) (see Table 1), voxels are then categorized as filled, occluded (hidden), empty (open), or unobserved.This concept is illustrated in Figure 2, where the voxel traversal and classification approach is schematically visualized for two laser pulses emitted from an ULS drone from two different viewpoints. Note that, in contrast to empty space, unobserved space cannot be explored because no laser pulses

are emitted in this direction. Such volumes should be mitigated by a well-designed scan setup and ideally account for a negligible volume fraction. The voxel traversal approach and classification scheme by Bienert et al. (2010) is just one possible way to map occlusion. Alternative approaches are further discussed in Section 3.5. Apart from mapping occluded voxels, aggregating statistics can provide a quick indication on the total observed volume in relation to the total analysed forest volume, which can help in assessing the representativeness of the laser acquisition. Equation (1), for instance, calculates the fraction of occluded volume in relation to a reference volume, which is usually defined by the space between the ground and the top of the canopy.

$$OcclusionFraction = \frac{OccludedVolume}{ReferenceVolume} \tag{1}$$

The challenge here lies in the definition of $ReferenceVolume$, since this is not always easily acquired. Above canopy acquisitions from e.g. ULS or ALS are able to define the reference volume quite accurately, since they are often well capable to derive accurate information on the terrain as well as the canopy surface. For ground-based acquisition, this becomes more error-prone. For example, even TLS acquisitions with a dense scanning pattern and under optimal leaf-off conditions still experience occlusion, especially in the upper part of the canopy. Additionally, so-called ghost beams (see Section 3.5) can hinder an accurate definition of the upper end of the canopy,

Table 1: Voxel classification scheme according to Bienert et al. (2010). Voxels are classified based on the number of hits (i.e. returns) in the voxel, the number of misses (i.e. penetrations that did not generate a return) and occlusions (i.e. rays that could have observed the voxel, but were blocked by other objects closer to the sensor).

	Number of		
	hits (N_{hit})	misses (N_{miss})	occlusions (N_{occ})
Filled	> 0	$\geqslant 0$	$\geqslant 0$
Empty	$= 0$	> 0	$\geqslant 0$
Occluded	$= 0$	$= 0$	> 0
Unobserved	$= 0$	$= 0$	$= 0$

even with a very dense scanning pattern. A common solution for ground based acquisition to receive an accurate $ReferenceVolume$ is to use additional above canopy acquisitions from either ULS acquisitions or TLS acquisitions with an above canopy vantage point (e.g. a crane or tower) (Schneider et al., 2019b) or from ALS (Kükenbrink et al., 2025). Though, essential here is that the time difference between the acquisitions is not too long. Virtual laser scanning could also help in defining the $ReferenceVolume$ (see Section 5.6 for further discussion on this topic).

3. Causes of occlusion and strategies for mitigation

Occlusion in forest environments can never be entirely avoided, and a fully representative 3D reconstruction of a scene is likely unachievable. The magnitude and spatial occurrence of occlusion depend on multiple factors: Firstly, the vegetation structure (i.e., the structural complexity, the density and the spatial arrangement) defines the setting for laser scanning. Secondly, the data acquisition strategies influence the actual resulting occlusion. Thirdly,

the technical properties of the laser scanning system (i.e., beam divergence and supported pulse rates) determine the theoretical capabilities of sampling the 3D space. Some of these factors follow general rules, while others are platform-specific. Additionally, mapping and quantification of occlusion depend on the chosen definitions and methods. While not directly linked to the cause of occlusion, these factors must be considered for its analysis as well. The following subsections provide a brief overview on occlusion causes and mitigation strategies, starting with general considerations on forest structure, followed by data acquisition parameters and strategies, implications of laser beam properties and methodological considerations. Table 2 provides a summary of technical laser scanning properties and their expected effect on occlusion. This section particularly addresses readers new to laser scanning in forests and those with an interest in optimizing field campaigns by further providing actionable guidelines for mitigating occlusion in Section 3.4 and Table A.5.

3.1. Forest structure and complexity

The specific forest structure sets the framework in which the effects of laser beam properties (see Section 3.3) and data acquisition strategies (see Section 3.2) need to be elucidated. The density and structural complexity of vegetation largely determine the degree of occlusion in relation to the scanner's position. The size of vegetation elements influences which type of occlusion dominates: small fragments such as leaves are prone to sub-

footprint occlusion, being easily missed during sampling or producing only partial beam reflections, while larger elements such as tree trunks more often cause geometric occlusion. The denser the spatial arrangement of vegetation elements, the higher is the likelihood of beam interception and consequently occlusion. Phenology in deciduous forests causes a high seasonal variability of structural density, whereby laser scans are much more affected by occlusion under "leaf-on" than under "leaf-off" conditions. Among all forest types, the dense structure of evergreen tropical rain forests poses the greatest challenge for scan completeness. In general, prior knowledge on forest structure such as the density and spatial arrangement (e.g., plantation forests following a regular grid) is highly beneficial and can be incorporated into data acquisition strategies to reduce occlusion.

3.2. Data acquisition parameters and strategies

Sampling density describes the number of laser beams used to sample a given volume. It is influenced by sensor properties and data acquisition strategies (see Table 2). An increased sampling density achieves a higher spatial resolution and exploitation of small gaps in the forest structure. This results in a more comprehensive exploration of space and reduction of occlusion (Gassilloud et al., 2025). The primary feature of laser scanners to affect sampling density is the pulse repetition rate (PRR), which has increased in recent years in commercial systems. While for many systems the PRR is fixed, for some it can be varied by the user (usually forming a trade-off with

the pulse energy and thus the maximum measurement range). Nevertheless, the blocking of beams through an object cannot be overcome by a higher sampling density from the same viewpoint. Instead it may lead to redundant sampling of known space with limited benefits on occlusion reduction. Therefore the main acquisition strategy to increase sampling density typically incorporates scanning from new viewpoints.

Viewpoints are the positions from which a sensor can sample space with its respective field of view (FOV). An increased number and optimized spatial arrangement of viewpoints is the fundamental approach to reducing geometric occlusion in any LiDAR scan (Brede et al., 2022; Gassilloud et al., 2025). Ideally new viewpoints can observe areas that were occluded from previous viewpoints.

For **above-canopy** flying ALS and ULS, the primary challenge is to overcome the blocking effect of the canopy. Figure 3 shows an example of point clouds and occlusion patterns for ULS surveys under both leaf-off and leaf-on conditions. While the system is able to penetrate relatively well into the canopy under leaf-off conditions, it encounters more occlusion in the lower part of the canopy caused by the dense foliage in leaf-on conditions. The coniferous trees which dominate on the left side of the depicted transect clearly show a high amount of occlusion for both acquisitions, whereas the deciduous trees dominating the right side of the transect show an increased amount of occlusion under leaf-on conditions. This demonstrates the phenological and forest type dependent variations in occlusion patterns

(Section 3.1).

The most effective strategy to reduce occlusion is to increase the number of new viewpoints by adding additional flight lines. If there are no preferences on domain-specific sampling, configurations are typically chosen to achieve uniform sampling and viewpoint distribution over the area of interest. This is usually realized by a regularly arranged grid of flight lines, i.e., regularly spaced parallel flight lines, crossed by a 90° rotated second set of lines, which can be complemented by a second double grid rotated by 45° (Brede et al. 2022; Gassilloud et al. 2025). If the sensor's FOV can be adapted, it is recommended to utilize the maximum possible scan angles (Gassilloud et al., 2025), while ensuring that scanner range limits are not exceeded at flight line edges.

The interplay between scan angle, flight altitude, and acquisition cost represents a critical trade-off in airborne survey design. Wider scan angles increase viewing direction variations and improve oblique canopy penetration, but increase the range to the target at flight line edges, enlarging the laser footprint and attenuating pulse energy (Hopkinson, 2007; Næsset, 2009; Morsdorf et al., 2008). Similarly, higher flying altitudes improve areal efficiency but increase beam travel distance which reduces pulse power per unit area through beam divergence and a reduced sampling density due to greater spacing between consecutive pulses. While lower flight altitudes mitigate these issues, this reduces the sensor's FOV overlap if no additional flight lines are added. Ensuring sufficient FOV overlap therefore increases acqui-

sition time and cost. Kükenbrink et al. (2017) recommended a lateral flight strip overlap of at least 50% for ALS campaigns to guarantee that every point in space is observed from at least two viewing directions. For ULS campaigns, much higher FOV overlaps are usually recommended and possible (e.g. Brede et al., 2022; Gassilloud et al., 2025). Optimizing this trade-off therefore requires balancing expected completeness gains against acquisition costs, ideally informed by prior knowledge of forest structure (e.g. canopy height, stand density, forest type).

For **ground-based laser scanning** acquisitions, occlusion is typically found towards the top of canopy, within dense tree crowns, and in dense understory vegetation. Figure 4 shows an example of point clouds and occlusion patterns resulting from ground-based laser scanning under leaf-off and leaf-on conditions for the same transect as also shown in Figure 3. The leaf-off TLS acquisition exhibits only minimal occlusion within tree trunks and towards the top of the crowns of coniferous trees, thanks to optimal sensor specifications (multi-return, narrow beam-divergence) and dense scanner placement (10 m maximum distance between scanner positions). The handheld MLS acquisitions suffer more from occlusion towards the canopy top, also for deciduous trees (right side of the transect), as the single-return system with a larger beam footprint, compared to the TLS system, struggles to penetrate through the denser part of the upper canopy.

For multi-station TLS surveys, occlusion is primarily controlled by the instrument positioning and by sensor settings. Viewpoints are limited to the

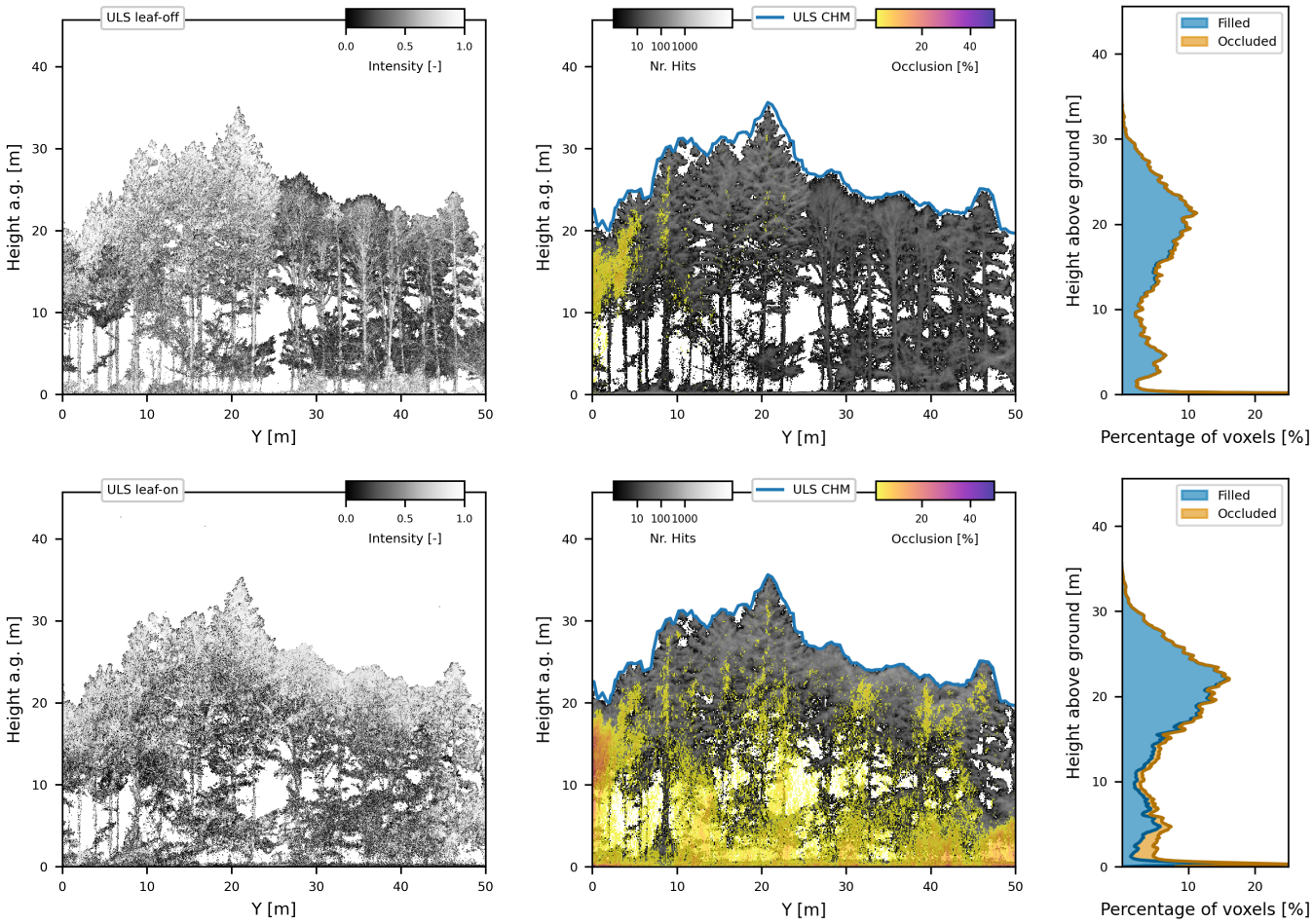

Figure 3: ULS point cloud (left, points coloured based on normalise laser return intensity) and occlusion example for leaf-off (top-row) and leaf-on (bottom) for a 10 m deep transect acquired using a RIEGL miniVUX-3 scanner. The middle column shows the percentage of occluded voxels in relation to the transect depth. Right column shows the cumulative profiles for occluded and filled voxels. White space denotes empty voxels, adding up to 100% of the canopy volume.

combination of single scan positions, and their spatial density and strategic placement are the key elements for reducing occlusion. However, station setup and potential target placement to aid scan-station registration are time intensive. Therefore, researchers aim to optimize sensor positioning to either

retrieve the best possible result with a given number of scans (Abegg et al., 2017; Wilkes et al., 2017) or to increase the number of scan positions just to the amount where the desired result can be obtained (Li et al., 2020). Often, a regular grid for sensor placements is chosen (Wilkes et al., 2017), due to a lack of prior knowledge on forest structure and better target visibility for co-registration. This strategy is supported by observational evidence (Wilkes et al., 2017) as well as simulations (Abegg et al., 2017). When the forest structure is known in advance, scan positions can be iteratively determined and optimized to efficiently cover occluded areas (Li et al., 2020).

Ground-based MLS surveys share similarities to multi-station TLS surveys in terms of point and occlusion distribution within the canopy. However, compared to TLS acquisition, due to its mobile acquisition strategy of MLS, it is easier to add further viewpoints by moving around the acquisition area. Various acquisition patterns have been reported in previous studies. Their selection is often strongly defined by the shape of the evaluated plot, resulting in a circular acquisition pattern for circular plots, whereas a grid-like pattern is typically employed for rectangular plots. Various variations of these two main approaches were reported by adding petal-like patterns to the acquisition (e.g. Gollob et al., 2020) or through the addition of more parallel lines and directions to the grid patterns (e.g. Mokroš et al., 2021). Sofia et al. (2024) reported that a star-shaped acquisition showed better performance for the estimation of canopy height compared to grid-shaped acquisitions due to the higher number of viewing angles.

Recent advances in robotics are also driving interest in under- and within-canopy drones for forestry applications. Although initial under-canopy drone laser scanning experiments date back to 2013 (Chisholm et al., 2013), most subsequent work has focused on manual acquisition in structurally simple, single-layered stands (e.g. Hyyppä et al., 2020). Liang et al. (2025) identify canopy complexity as one of the main obstacles to under-canopy ULS, alongside trajectory planning, limited GNSS coverage beneath the canopy, and autonomous obstacle avoidance. As robotic obstacle avoidance improves in complex environments such as forests, a wider deployment of under-canopy drones is likely to become feasible in the near future. Autonomously flying ULS would then offer far greater viewpoint flexibility, potentially combining under-, within-, and above-canopy perspectives automatically, and thereby substantially reduce occlusion (see also next paragraph).

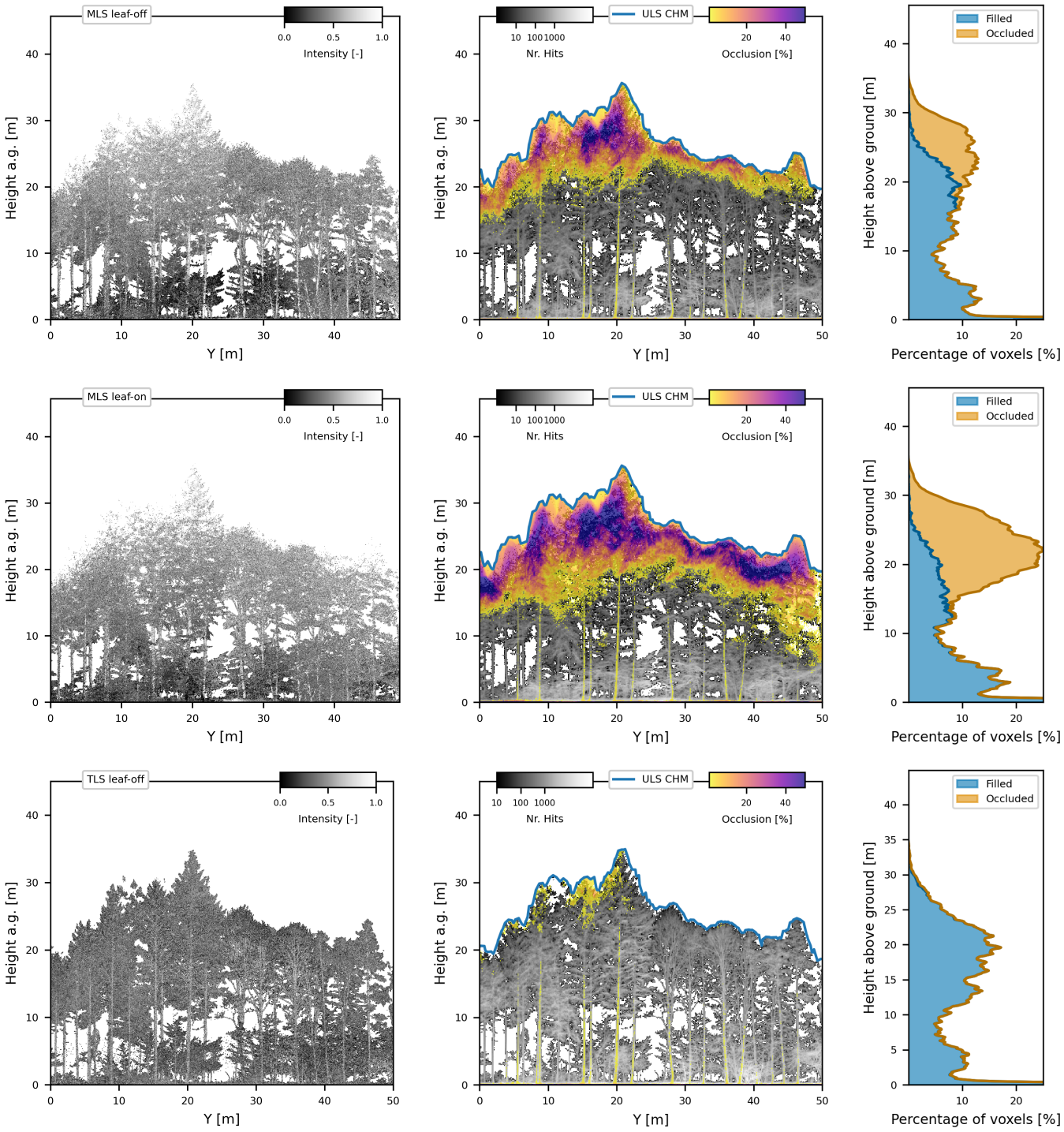

Figure 4: Ground based laser scanning point cloud (left, points coloured based on normalised laser return intensity) and occlusion example for MLS leaf-off (top-row), MLS leaf-on (middle), both acquired using a GeoSLAM ZebHorizon handheld scanner, and TLS (bottom - RIEGL VZ400i) for a 10 m deep transect. The middle column shows the percentage of occluded voxels in relation to the transect depth. Right column shows the cumulative profiles for occluded and filled voxels. White space denotes empty voxels, adding up to 100% of the canopy volume.

Currently, the best way to reduce geometrically occluded areas is the **combination of multiple perspectives** from above and below canopy, as they complement each other. Schneider et al. (2019a) demonstrated that occlusion could be reduced to <2% with a combination of ground and above canopy laser scans in tropical and temperate forests. This is also shown in Figure 5 where the leaf-on MLS and ULS acquisitions shown in Figures 3 and 4 were combined in order to reduce the areas of occlusion of the respective acquisitions. Therefore, also fusion of TLS and ULS has been proposed in recent studies (Terryn et al., 2022; Yrttimaa et al., 2020). Another approach is scanning at different heights (e.g. via poles, scaffolds or canopy cranes) which can enhance penetration especially in the crown area (D'hont et al., 2025; Schneider et al., 2019a; Yun et al., 2019). However, these combination and fusion methods come with the challenge and errors of co-registering the scans from different viewpoints and potentially different systems.

These general strategies for mitigating geometric occlusion come with limitations, as some parameters form complex inter-relationships and have a direct impact on others. Furthermore, logistics and budget typically constrain the acquisition time, so that acquisition patterns need to be optimised. For ALS and ULS, acquisition time is limited by flight time restrictions (e.g. battery capacity). For MLS devices which are reliant on simultaneous localization and mapping (SLAM) technology, prolonged and more complex acquisitions could potentially result in issues with misalignments and drifts within the acquired point clouds (Kükenbrink et al., 2025; Mokroš et al.,

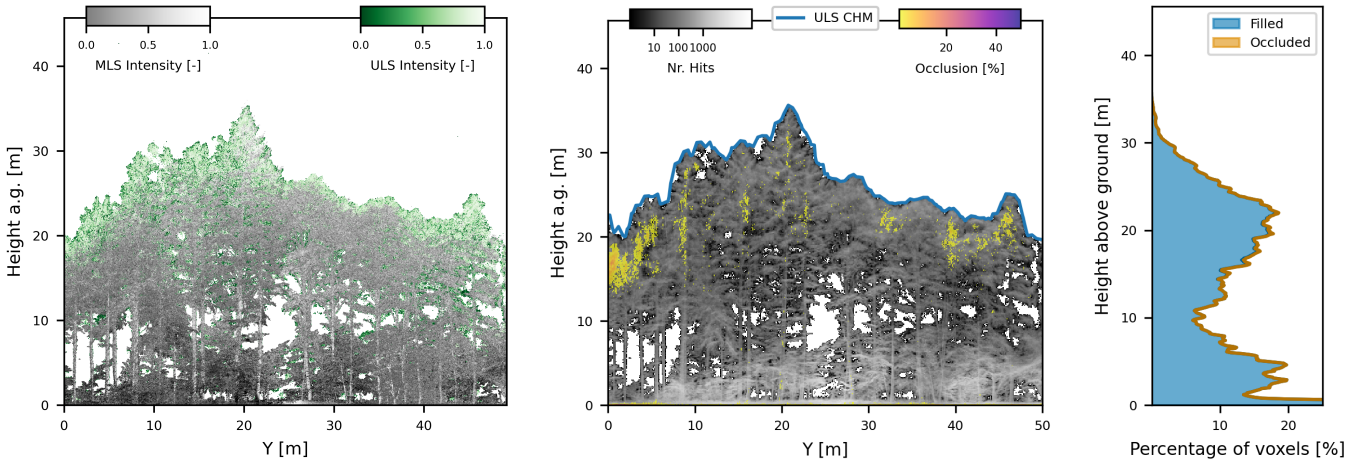

Figure 5: Point cloud and occlusion pattern example for a combination of MLS (GeoSLAM ZebHorizon) and ULS (RIEGL miniVUX-3) acquisitions under leaf-on conditions. The below and above canopy vantage points complement each other to produce a point cloud with minimal occlusion. Individual acquisitions are shown in Figure 3 for ULS acquisition and in Figure 4 for MLS acquisition

2021). Moreover, increased acquisition time for any laser scanning platform may lead to stronger effects from wind-induced vegetation movement, and additional viewpoints result in more frequent co-registration errors.

3.3. Laser beam properties

Laser beam properties are usually not changeable but need to be kept in mind since they impact the processes of beam-canopy interaction including sub-footprint occlusion. For the same forest structure, occlusion patterns will differ depending on the beam properties (Brede et al., 2022). The main scanner parameters to consider are beam divergence (including beam exit diameter), beam energy, wavelength, pulse duration and the capability to record multiple returns (Table 2).

Abegg et al. (2021) found that for TLS, small objects are less occluded when scanned with smaller beam diameters. Larger beam diameters and hence larger beam footprints often cause multiple objects to be hit by the laser pulse, favouring the identification of the larger objects in the footprint which reflect more energy as well as lowering the spatial accuracy of the generated return (Abegg et al., 2021).

On the other side, at least for multi-return systems, larger beam diameters result in more points per pulse and therefore reduce the geometric occlusion of canopy objects that lie in the line of sight of the emitted beam (Abegg et al., 2021). For such multi-return scenarios, assuming the same footprint size, higher beam energy allows for a higher number of targets, since the cross section of each target decreases with increasing number of targets as the energy is distributed on them (Wagner et al., 2008). Higher beam energy allows detection of more targets by keeping individual returns above the detection threshold, even as the reflected energy of each return weakens with more targets (Wagner et al., 2008). If the energy cross section falls below the threshold of the detector, targets hit by the laser beam cannot generate a return and are therefore occluded.

Finally, the range resolution (shortest separation of objects that can be measured) can result in sensor-specific occlusion of canopy objects. If objects lie within the dead zone from the previous return, they cannot be detected (Wagner et al., 2008), leading to censoring of potentially detectable features (Bai et al., 2026). Effects of beam divergence, pulse power, pulse duration

Table 2: Laser scanning sensor specifications and their effect on occlusion when increasing the laser scanning specification.

Category	Specification	Definition	Affected properties	Effect on occlusion
Data acquisition parameters	Angular resolution [°]	Angular distance between consecutively emitted laser beams	Sampling density	↓
	Pulse repetition rate [kHz]	Number of pulses sent out per unit of time	Sampling density	↓
	Platform speed [m/s] or [°/sec]	Movement speed of the platform (ALS/ULS/MLS) or rotational speed of the scanner head (TLS)	Sampling density	↑
Laser Beam Properties	Wavelength [nm][a]	Wavelength of the emitted laser light	Target reflectivity/ absorption, return energy, number of returns	↓ ↑
	Pulse energy [nJ]	Energy of the outgoing pulse	Beam energy distribution, number of returns	↓
	Beam divergence [mrad]	Angular increase in footprint diameter with distance from the aperture	Footprint size, beam energy distribution, multiple returns	↓ ↑
	Pulse duration [ns]	Length of time for a single pulse to be emitted	Minimal detectable distance	↑

[a] The effect of wavelength on occlusion is non-monotonic and depends on the wavelength-specific absorption and reflectivity of the target material (e.g. foliage water content). For instance, SWIR wavelengths near water absorption features yield weaker returns from moist foliage, whereas NIR wavelengths fall within the high-reflectance plateau of vegetation.

and other laser scanning specifications and their interaction are described in more detail by Morhart et al. (2024), Roussel et al. (2017) and Wagner et al. (2008) based on field experiments, and Abegg et al. (2021), Disney et al. (2010) and Hancock et al. (2015) based on simulation studies.

3.4. Practical guidance across forest types and platforms

Building on the causes and mitigation strategies discussed above, we condense our recommendations into actionable best practices for laser scanning acquisition campaigns across a range of forest types and platforms. As established in Section 3.2, increasing the number of viewpoints, including by fusing

below- and above-canopy acquisitions, is the most effective way to minimise occlusion, but this always has to be weighed against acquisition time and, ultimately, cost. Beyond a certain point, additional viewpoints yield more redundant structural information rather than improved canopy observation, so that their benefit no longer justifies the added cost (e.g. Abegg et al., 2017; Boucher et al., 2021; Torralba et al., 2022).

Detailed, platform- and forest-type-specific guidelines, covering acquisition design, occlusion hotspots, mitigation priorities, and the corresponding reporting conventions we recommend, are provided in Appendix A with Table A.5. In all cases we recommend that occlusion is routinely quantified and reported alongisde derived structural metrics, and treated as a formal quality flag for those most sensitive to it. This is especially critical in time-series contexts, where between-acquisition differences in occluded volume can masquerade as real structural change (see Section 5.4).

3.5. Impact of methodology on occlusion mapping and quantification

Mapping occlusion seeks to spatially identify and quantify both explored and unexplored volumes. This is a difficult task, since for an extensive understanding of occluded space, modelling the physical interaction between laser beams and intercepting objects is required. This needs fundamental knowledge on beam properties, such as the energy distribution within a diverging beam, and detailed object characteristics, such as their spatial location, orientation, surface roughness, and optical properties. However, the point cloud

is often the only information available, which is insufficient for the accurate reconstruction of laser-object interactions.

Therefore, simplified approaches that trace the trajectory of emitted laser beams through space are commonly used to quantify occlusion. Along the trajectory of a laser pulse, it is necessary to determine whether the beam traveled through empty space, was partially reflected by objects (returns), or reached a point beyond which no or insufficient energy was returned to the sensor (occlusion). The volume, which was traversed by laser beams, can then be mapped according to these respective states. Voxel-based ray tracing algorithms are highly suited for this task, as they allow a very efficient and convenient classification of three-dimensional space and the retrieval of aggregated statistics (see Figure 2 for an illustration of the voxel traversal mechanism).

To map occlusion, emitted laser pulses must first be reconstructed as vectors from their origin to the last return. Thus, knowing the pulse origin, typically given by scan position or trajectory data, is essential for both static and mobile laser scanning systems. If sensor positions are available for mobile acquisitions, the link between laser returns and its respective pulse origin is usually performed through a time flag (i.e. GPS time) available both in the trajectory and the point cloud. By extending the beam vector beyond the last return of the pulse, the occluded part of the laser pulse can be identified. By extending the beam vector beyond the last return of the pulse, the occluded part of the laser pulse can be identified. The provision of sensor positional

information is, however, still not standard and can be missing altogether; we discuss the implications of this, and approaches to reconstruct positions directly from the point cloud, in Section 4.2.

Voxel-based ray tracing algorithms divide space into a 3D grid of voxels. While many approaches mapping occlusion in a voxel grid follow a binary classification scheme (see also Section 2), other approaches describe voxels with fuzzy membership functions to provide a more comprehensive picture (Béland et al., 2011). Those can be used to identify voxels that are "under-sampled" for specific tasks such as leaf area density (LAD)/PAD estimations (see Section 5.3), where a minimum sampling of space is required to retrieve reliable metrics.

Essential for all voxel-based occlusion mapping approaches is the definition of the dimensions of the voxels. The voxel size is a question of scale and has a strong impact on how much of the voxel grid is potentially quantified as occluded (Kükenbrink et al., 2017). With a voxel size too small, many voxels of a grid would potentially not be traversed by laser scanning beams, which subsequently leads to their classification as "unobserved". A voxel size too large hampers the detection of occlusion since larger voxels are more likely to be traversed by beams and therefore be classified as "observed" or "filled". A balanced voxel size enables meaningful analysis and helps identify occluded areas. As a general rule, the voxel size should be considerably larger in linear dimension than the beam width so that they effectively represent the information generated by the scanner. For ALS, a voxel size of 1 m was

found to be beneficial (Kükenbrink et al., 2017), while studies investigating high-resolution laser scans with TLS or ULS commonly use a voxel size of 10 cm (e.g. Brede et al., 2022; Kükenbrink et al., 2017; Kükenbrink et al., 2025; Gassilloud et al., 2025; Schneider et al., 2019a). The proportion of volume occluded is therefore not only an intrinsic property of the structure and the scanning parameters but also of the subsequent data processing.

Voxel traversal algorithms are straightforward to use but have certain limitations, as they simplify the underlying reality. Due to the inherent beam divergence, LiDAR beams observe larger volumes with increasing distance from the sensor. However, beam trajectories are commonly treated as (infinitesimally small) lines, and the beam divergence is not taken into account. Therefore, the actual explored volume of a LiDAR beam is not captured, and the occurring occlusion is overestimated (Kükenbrink et al., 2017).

Especially for ground-based laser-scanning approaches, empty pulses (i.e. pulses that did not trigger a laser return) can occur, when laser pulses are emitted through canopy gaps into open sky. This is less of a problem for ULS or ALS acquisitions, as generally every laser pulse will generate at least one return when reaching the ground at the latest. Not accounting for pulses without returns can result in an overestimation of occlusion and unobserved space. These pulses are absent from point clouds, and often difficult or impossible to extract from raw data of commercial scanners. Moreover, it is generally not possible to distinguish true gaps (where pulses yield no returns) from instances where returns are missing due to instrument-based filtering,

where the return signals fall below the scanner's detection threshold. In (Schneider et al., 2019a), the extent of overestimation due to not modelling these pulses is investigated in both a temperate and dense tropical forest. They showed that the overestimation is data-dependent, but limited in both forests, and potential bias introduced by misclassifications and modelling of near-scanner obstructions as gaps would likely be worse.

This leaves room for improvement and opens up several opportunities for the development of new methods. Future studies might move away from aggregating statistics in a voxel grid and come towards a quantification of "true" observed and occluded volume. This will include the consideration of an (unequal) beam divergence to assess the actual volume explored by the individual laser beams. Further, the energy and its spatial distribution within the laser beam could be taken into account. Assessing the fraction (both energy and footprint) of reflected laser beams as well as the remaining pulse fraction further traveling along the pulse direction has the potential to discretely quantify the occluded 3D space for each laser pulse. Incorporating full-waveform information could further improve the quantification of the 'true' occluded space, as it provides more detailed insights into pulse-target interactions than the discrete returns derived from the waveform. However, only selected devices (e.g. Riegl VZ-400i with enabled optional full-waveform capabilities for TLS) actually allow for an analysis of the full-waveform information. Additionally, due to significant storage overhead and data complexity of the full-waveform information, this information is currently often

disregarded, even when available.

4. Occlusion tools

Currently, there are only a few tools available for performing occlusion mapping. Three of these tools were presented at the SilviLaser conference 2023 in London (Brede et al., 2023). The available tools show various stages of implementation, ranging from Python (*OccPy* and *CANOPy*) or R (*voxelizeR*) packages up to stand-alone software tools and plugins with a fully functional GUI (*AMAPVox* and *L-Vox*), making it easy for the user to find a suitable tool for their needs. In Table 3 and the following section we present five software tools for occlusion mapping. Other software capable of performing occlusion mapping tasks may exist but have not been tested and evaluated by the authors.

4.1. Occlusion mapping software tools

AMAPVox was initially developed as a stand-alone Java application including a GUI for easy user interaction (Vincent et al., 2017). Since a few years, an R package has been implemented as an interface to the Java based core code. AMAPVox was developed for the estimation of vegetation densities (i.e., PAD/LAD, plant area index (PAI)/LAI), but its voxel-grid based outputs can be used to create 3D occlusion maps. The tool traces each laser pulse through a pre-defined voxel grid and computes the local transmittance or attenuation for each voxel, from which occlusion information can be retrieved and visualized.

OccPy is a python package where the computationally heavy processing is performed through a C++ implementation of the voxel traversal algorithm introduced by Amanatides and Woo (1987). The interface between the Python and C++ code base is realized through Cython. The tool was initially implemented as Matlab scripts to map occlusion (Kükenbrink et al., 2017) and to estimate vegetation densities from ALS acquisitions (see Table 3 for links to the different tool versions). Later, it was optimized to map occlusion from various platforms and translated into a python package called OccPy.

VoxelizeR is implemented in the R statistical programming language (Brede et al., 2025). It computes the laser's trajectory intersection with the grid lines of the defined voxel grid independent in the three grid dimensions (Brede et al., 2022). It was developed for PAD estimation and occlusion analysis, and interfaces with R's *lidR* and *sf* packages.

CANOPy is a recently published and customizable occlusion mapping tool implemented in Python. It was originally developed for the study in Gassilloud et al. (2025). It is capable of reconstructing sensor position trajectories from point clouds with multiple returns. The module has implemented a box intersection algorithm (Williams et al., 2005) to limit ray tracing to an area of interest and uses the voxel traversal algorithm by Amanatides and Woo (1987).

L-Vox is a plugin for the open source, collaborative platform for remote sensing data processing in a forest context Computree (Computree

Core Team, 2024). Similarly to AMAPVox, the main purpose of L-Vox is the estimation of PAD, but unlike AMAPVox, L-Vox is specialized to handle TLS scans only. L-Vox is also based on the voxel traversal algorithm introduced by Amanatides and Woo (1987) and can map occluded voxels alongside estimated PAD. L-Vox further implements an occlusion mitigation step to fill in occluded voxels with the average PAD of the respective vertical layer (see also Section 5.2 and Section 5.3). Since L-Vox is designed as a plugin for Computree, no scripting or programming knowledge is necessary for execution.

4.2. On the importance of scan locations and trajectory information for occlusion mapping

For successful occlusion mapping, the trajectory of each laser pulse must be reconstructed from its origin and at least one return (Section 3.5), which makes knowledge of the sensor position throughout the acquisition essential. Yet such positional information is still not routinely archived. We therefore strongly recommend that all users store scanner positions (for TLS) or trajectory information (for mobile acquisitions, e.g. ULS, MLS) alongside the acquired point clouds, as these are often a standard export option of the processing software. Where the information is missing, or where platform trajectories do not adequately represent the sensor position (e.g. for a LiDAR mounted on an offset gimbal), it can in some cases be reconstructed from the point cloud itself (e.g. Gassilloud et al., 2025; Kükenbrink et al., 2017), and

several of the tools introduced above implement such functionality: CANOPy reconstructs sensor trajectories from multi-return point clouds,while the L-Vox plugin infers the scanner location geometrically from the common origin of all pulses in a single TLS scan, but is therefore restricted to TLS and cannot be applied to MLS, ULS or ALS acquisitions. Because all of these approaches rely on either multi-return pulses or a static scan origin, they introduce additional uncertainty in the estimated positions and are no substitute for recording them directly.

Table 3: Five examples of occlusion mapping software tools with different implementations

Criteria	**AMAPVox[1]**	**OccPy[2]**	**voxelizeR[3]**	**CANOPy[4]**	**L-Vox[5]**
Height normalisation	Yes	Yes	Yes	Yes	Yes
3D plotting outputs	Yes	Yes	No	Yes	Yes
Beam size consideration	Yes	No	No	No	No
Multi-core processing	Yes	Yes[a]	Yes[b]	Yes	Yes
Multiple inputs[c]	No[d]	Yes	Yes	Yes	No[d]
Mobile-compatible (MLS/ULS)	Yes	Yes	Yes	Yes	No
LAD-relevant metrics	Yes	Yes[e]	Yes	Yes	Yes
Graphical user interface	Yes	No	No	No	Yes
Manual / vignette	Yes	Yes	Yes	Yes	Yes
Test script available	No	Yes	Yes	Yes	No
Required software	R, AMAPVox	Python, Cython, Conda	R, QGIS	Python, Conda	Computree
Ease of installation	Easy	Easy	Easy	Easy	Easy
Operating system	U/W/M	U/W/M	U/W[b]	U/W	U/W/M
Input formats (point cloud)	`.las/.laz`, `.rxp/.rsp`, `.ptx/.ptg`, `.xyb`, `.sht`	`.las/.laz`, `.rxp/.rsp`	`.las/.laz`	`.las/.laz`	`.las/.laz`, `.ply`, `.xyb`, `.csv`, `.ptx`
Input format (Scan Pos./Trajectory)	`.csv`	`.csv`	`.traj`	`.csv`, `.gpkg`	NA[f]
Output format	`.vox`	`.npy`	`.tif`	`.npy`	ASCII grids
Reference	Vincent et al. (2017)	Kükenbrink et al. (2017); Schneider et al. (2019a)	Brede et al. (2022)	Gassilloud et al. (2025)	Nguyen et al. (2022)

Operating system: U Unix, W Windows, M macOS. [a]Multi-core on Windows. [b]Multi-core on Unix only. [c]Multiple point clouds or trajectories. [d]Possible via repeated execution for different TLS scan stations. [e]Not in OccPy (Python); available in the Matlab version. [f]Scan position inferred geometrically from TLS scans; not compatible with mobile acquisitions.

Software/repositories: [1] `https://amapvox.org`; [2] `https://github.com/dkueken/OccPy` (Python), `https://www.eufar.net/documents/6028/` (Matlab); [3] `https://doi.org/10.5281/zenodo.16759585`; [4] `https://github.com/MGEOS/CANOPy`; [5] `https://computree.onf.fr/`.

5. Research opportunities through occlusion mapping

Rather than solely treating occlusion as a challenge to be overcome, occlusion metrics and mapping can be viewed as an informative feature of acquired point clouds and for assessing vegetation structure. Taking occlusion into account allows to improve the accuracy of forest metrics, providing a more realistic appraisal of measurement uncertainty, and opens up new perspectives on how forest structure can be sampled or studied. In this section, we will discuss various research opportunities highlighting the potential of occlusion mapping for a range of applications.

5.1. Occlusion mapping for smart, autonomous LiDAR data acquisition

During data acquisition, canopy discovery and scan completeness always have to be balanced with scanning time and available personnel, while also avoiding redundancy in collection. Some general guidelines have emerged to achieve this, e.g., regular grid patterns for TLS (Wilkes et al., 2017) and multi-directional grid flight lines for ULS (Brede et al., 2022; Gassilloud et al., 2025). However, while grid patterns appear as intuitively optimal and generally result in a good discovery throughout the area of interest, they do not adapt to spatially variable occlusion. Their implementation is typically time consuming, as the grid size will be chosen conservatively with a focus on the densest forest parts. A few scanning hardware products with live previews already exist, e.g., RIEGL scan map for the VZ-i series (TLS), FARO Stream application for FARO Orbis (MLS), and DJI Pilot application

for DJI Zenmuse L2 or L3 (ULS). However, they only give an indication of completed areas and preview point cloud density. Point cloud density does not help to indicate the degree of exploration for specific volumes like the crown layer, and empty and occluded spaces cannot be differentiated in point density maps. Here, occlusion mapping could serve as a guidance for efficient data acquisition with completeness in mind. Li et al. (2020) proposed an iterative scanning mode, that optimizes scan positions for maximum volume exploration, aiming at an adaptation to local conditions. Even though this approach only follows a simplified task of detecting trunks at breast height or simplified, circular crown shapes on a horizontal plane while assuming known tree positions, it highlights the future potential with respect to adaptive scan planning.

Recent advances in robotic navigation allow mobile legged robots equipped with LiDAR scanners to perform autonomous forest inventories along human-defined paths. Here, Chirici et al. (2023) showed that the accuracy of tree detection and derived DBH strongly depended on the selected acquisition path. Freißmuth et al. (2024) and Mattamala et al. (2024) presented an online, incremental processing pipeline using a mobile legged robot, allowing for visualisation of forest models during data collection. Such pipelines allow for live decision making and minimisation of occlusion through path modifications by the human operator. Moving one step further, Karjalainen et al. (2025) tested an autonomous below-canopy flying unoccupied aerial vehicle (UAV). An integration of explicit occlusion mapping into these solu-

tions could improve decision making of the operator, or could further be used for autonomous path planning and adaptation by autonomous platforms to optimize data coverage.

Ideally, a universal optimization approach should target full canopy exploration in order to be agnostic of later analysis objectives, produce results in 3D, and assume no prior knowledge of the forest stand. At the same time, it should take into account requirements for target-less registration between scan positions via point cloud features (e.g., sufficient overlap between individual data takes). Finally, redundant coverage should be minimised. Both registration and occlusion mapping could happen onboard and in real time (Eisoldt et al., 2025). Such an intelligent approach would allow actionable insights and significantly enhance efficiency in both static (i.e., TLS) and mobile laser scanning (i.e., MLS, ULS). Algorithms are becoming available (see Section 4) but to be operationally implemented for an on-the-fly occlusion mapping on the device, they must meet high performance standards and demonstrate robustness.

5.2. Quantification of uncertainty with occlusion mapping

Forest structure can be described by a variety of geometrical metrics such as tree height and DBH distribution, layering indices, fractal dimension, quantitative structure models (QSM), gap fraction and density metrics such as PAD or LAD. All of these metrics can be estimated from point clouds. Therefore, laser scans need to capture the targeted forest structures with

sufficient point density and spatial accuracy.

Currently, point cloud quality and feature representativeness are assessed 1) via sampling density or 2) by comparing point cloud geometries and derived metrics (e.g. DBH, above ground biomass (AGB)) with ground truth data (Dalla Corte et al., 2022; Neuville et al., 2021). Table 4 provides an overview of the severity of occlusion effects on various structural metrics, based on the authors' expert judgment. These are generalizing judgments for very broad categories. Therefore nuances within categories can be expected, mainly due to varying sensor characteristics (see Section 3.3) or data acquisition strategies (see Section 3.2). For example a TLS system capable of producing multiple returns per pulse may suffer less from occlusion for tree height estimation than a TLS system only capable of recording a single return.

While research investigates uncertainty from the perspective of what has been observed, occluded space is often disregarded. Even though the scientific community is aware of uncertainties resulting from occluded space, it is rarely quantified and made use of. Instead, studies tend to accept a certain degree of uncertainty in their data and usually do not recognize the potential of quantifying occluded space to set their work into the context of their laser scanning data.

Occlusion is widely discussed as a driver of bias in derived structural metrics: the systematic underestimation of canopy height from ground-based systems is a well-known example, as also illustrated in Figure 4, where below-

Table 4: Expert judgement of the severity of occlusion effects on different structural metrics (low *o*, medium +, high ++) in dependence of the utilized platform.

	Structural metric	Reference	TLS	MLS	ULS/ALS
Tree metrics	**Tree height**	Brede et al. (2017) Davison et al. (2020)	+	+	o
	DBH	Brede et al. (2017) Davison et al. (2020)	o	o	++
	Trunk volume/ stem curve	Prendes et al. (2021)	o	o	++
	Crown projection area	Panagiotidis et al. (2022)	o	o	+
	Crown volume	Panagiotidis et al. (2022)	+	+	+
	QSM	Hartley et al. (2024)	++	++	++
	Leaf area	Frey et al. (2025) Yun et al. (2019)	++	++	++
Plot metrics	**Canopy surface area (DSM)**	Heidrich et al. (2023)	+	+	o
	Canopy cover / gap fraction	Heidrich et al. (2023)	o	o	o
	LAI/PAI	Wang and Fang (2020)	++	++	++
	Occupied/open space	Jung et al. (2013)	+	+	++
	Vertical layering	Knuff et al. (2020)	o	o	+
	Box dimension	Mathes et al. (2023)	++	++	++

canopy laser scanning underestimates canopy height relative to ULS-derived heights due to the increased occlusion in the upper canopy. Yet this link is rarely made explicit by quantifying the occluded space and relating it to the magnitude and uncertainty of the resulting bias, as such a direct relation is often difficult to build. Schneider et al. (2019a), for instance, linked occluded volume with bias in PAD estimation, but could not validate this bias due to missing reference PAD measurements. Nevertheless, the most thorough treatment of occlusion-induced bias to date comes from work on vegetation density estimation, where voxel-scale PAD estimators have been analysed with explicit confidence intervals (Pimont et al., 2018) and their bias

assessed against reference scenes — whether simulated (Soma et al., 2021; Nguyen et al., 2022) or built from multi-station acquisitions of increasing scan density (Béland and Kobayashi, 2021). We discuss these in detail in Section 5.3. Extending such estimator- and uncertainty-aware assessment to the broader set of metrics in Table 4 remains an open opportunity.

We see quantification of occluded space as a promising tool to identify data gaps, assess uncertainty, and highlight potentially omitted structures. Therefore it has great potential to evaluate point cloud and feature representativeness and link missing information to possible errors of derived metrics. Future studies should further invest in the evaluation of how occluded space affects estimated forest structural variables and their uncertainties.

5.3. Vegetation density metrics

Estimating vegetation densities is crucial for understanding vegetation structure and function in ecological studies. The 3D distribution of vegetation can be described by LAD or — in case leaf and wood material cannot be discriminated — PAD. These parameters have been estimated through various methods based on a similar theoretical background which describes the exponential attenuation of transmittance in a uniform medium along the path of a laser beam, also known as Beer's law (Béland et al., 2011; Pimont et al., 2018; Soma et al., 2021). Most models aiming to estimate 3D LAD or PAD follow a voxel-based approach (e.g. Vincent et al., 2017), in which the density within each voxel is inferred statistically from the fraction of laser

pulses intercepted relative to the number entering it. The accuracy of such estimators, and, for sparsely sampled voxels, their bias, therefore depends directly on the per-voxel sampling, which is exactly what occlusion reduces. Pimont et al. (2018) made this link explicit by deriving PAD estimators and confidence intervals at the voxel scale, showing that low sampling widens the confidence intervals and can bias the retrieved density. The per-voxel pulse statistics underlying occlusion mapping are thus the natural basis for flagging "undersampled" voxels and propagating these sampling limitations into the uncertainty of LAD/PAD (see Section 3.5). Several of the voxel-based tools presented in Section 4 (e.g. AMAPVox, L-Vox) were in fact originally developed for LAD/PAD retrieval, underlining the close methodological link between vegetation density estimation and occlusion mapping.

Empirically, this sampling-driven bias manifests as a significant underestimation of LAD or PAD in the upper part of the canopy for ground-based systems or in the lower part of the canopy for above canopy systems (Béland et al., 2014; Schneider et al., 2019a; Soma et al., 2020, 2021), since pulses are frequently occluded earlier along their path (Béland et al., 2014; Soma et al., 2018, 2021). The choice of voxel size is central to this bias and constitutes a genuine trade-off (see Section 3.5): a larger voxel increases the effective sampling rate, but Soma et al. (2021) demonstrated analytically through simulations that using larger voxels can in turn worsen underestimation, owing to the more heterogeneous distribution of vegetation within each voxel. They therefore suggested a voxel size of close to 0.5 m as a compromise for

TLS-based PAD/LAD estimation, whereas Nguyen et al. (2022), using the L-Vox estimator, reported an optimal size of approximately 0.1 m depending on foliage dimensions. Rather than contradicting each other, these results indicate that the optimal voxel size is not universal but depends on foliage dimension, vegetation heterogeneity, the chosen estimator and the laser scanning platform. The trade-off is further modulated by the laser beam itself: because beam divergence increases the effective volume explored with distance (see Section 3.5), treating beams as infinitesimal lines can bias both the occlusion estimate and the derived density, an effect that becomes more pronounced relative to small voxels.

A complementary strategy to mitigate biases in LAD or PAD estimation is to increase sampling density through a denser scanning pattern, i.e. by generating more viewing directions (Wilkes et al., 2017; Schneider et al., 2019a). Béland and Kobayashi (2021) showed for multi-station TLS that occlusion effects on LAD can be substantially reduced by increasing the number of scan positions. Consistently, Nguyen et al. (2022) found that multi-station TLS reduces occlusion induced bias in PAD compared to single-scan setups. Where additional viewpoints are not feasible, various approaches have been introduced to compensate biases due to insufficient sampling, ranging from a simple filling of occluded voxels with an average LAD or PAD of explored voxels at a given height (Béland et al., 2014; Nguyen et al., 2022; Schneider et al., 2019a), through more sophisticated kriging interpolation (Soma et al., 2020), up to light transmission (Béland et al., 2011) or architectural

(Côté et al., 2011) models. Yet, all these compensation approaches rely on the knowledge of the spatial distribution of occluded voxels, again highlighting the importance of occlusion mapping to gain insight into sampling and occlusion patterns.

Beyond correcting biases, occlusion mapping offers a route to explicitly quantify the uncertainty of derived density metrics (Section 5.2). Whereas statistical estimators already provide voxel-scale confidence intervals under sampling limitations (Pimont et al., 2018), their robustness to occlusion has so far been assessed mainly against simulated reference data: Soma et al. (2021) relied on controlled simulations, and Nguyen et al. (2022) benchmarked L-Vox against a reference numerical forest, reporting close agreement ($R^2 > 0.98$) while isolating the residual influence of occlusion. A persistent obstacle is the lack of an absolute reference for the "true" LAD/PAD, since even dense multi-station TLS acquisitions remain incomplete, and conventional indirect optical methods routinely used as a field reference (e.g. digital hemispherical photography and transmittance sensors such as the LAI-2000) give themselves biased results (Breda, 2003; Calders et al., 2018). Virtual laser scanning and reference numerical forests (see Section 5.6) offer a complementary route, since within the simulated scene the occupied volume and the target density are known by construction rather than estimated. This provides a controlled setting in which estimator robustness can be characterised and occluded volume can be quantified and linked to a bias in PAD (e.g. Nguyen et al., 2022; Yun et al., 2019), although the realism of the un-

derlying scene and sensor model sets a limit on how directly such results transfer to field data (see Section 5.6)

We have treated vegetation density in detail here as it is the structural parameter most directly tied to the voxel grid, but the same voxelization trade-offs, between voxel size, beam divergence and the resulting sampling, propagate into other voxel-derived metrics such as 3D (voxel-resolved) canopy gap fraction and structural complexity measures (e.g. box dimension or vertical layering; see Table 4 and Section 5.2). For these metrics the dominant risk is different. Rather than a sampling-driven density bias, the main problem is that occluded volume is mistaken for empty space, which inflates apparent gaps and distorts complexity estimates. Reliable interpretation therefore depends on distinguishing occluded from genuinely empty space (Section 2).

5.4. Time series analysis

In recent decades, most forest research involving laser scanning has focused on processing point cloud data and deriving forest and tree structural metrics from one time step. However, as multi-temporal laser scanning datasets become increasingly available, research is gradually shifting towards analyzing changes in these structural metrics over time (e.g. forest and tree structural dynamics). Despite increasing availability, quantifying forest dynamics and structural change from such data remains a complex and unresolved challenge. One of the key obstacles lies in the issue of data interoperability (Bartholomeus et al., 2022). Over the years, a wide range of

laser scanning sensors has been developed for various platforms, each with its own specifications and characteristics. As a result, data collected at different time points may have been acquired using different scanners (Huertas et al., 2022; Loh et al., 2022; Yin et al., 2024; Qi et al., 2023). Additionally, due to time constraints or optimized field protocols, data may have been gathered using coarser scanning grids or alternative settings (e.g., faster scanning speeds). Beyond these technical factors, the forest structure itself evolves over time due to seasonal variation (Figure 6), tree growth, and mortality, all of which can significantly affect point cloud quality in terms of a complete representation of the forest canopy. Point cloud quality in multi-temporal datasets can differ substantially, often due to a combination of technical factors and structural forest changes. As a result, point cloud completeness and occlusion can vary substantially between acquisitions of the same site over time, which can, in turn, affect the accuracy of detected changes.

Differences in errors associated with structural measurements from point clouds at different time steps are particularly critical when direct measurements are used (Loh et al., 2022; McRoberts et al., 2015). For example, if tree height is underestimated more in the first time step than in the second, the calculated change in tree height may be significantly overestimated. Therefore, differing occlusion characteristics pose a major challenge for this approach unless the effects of occlusion are properly detected, quantified, and incorporated into the analysis. In other words, the central challenge in time series analysis is to minimize the uncertainties involved in distinguish-

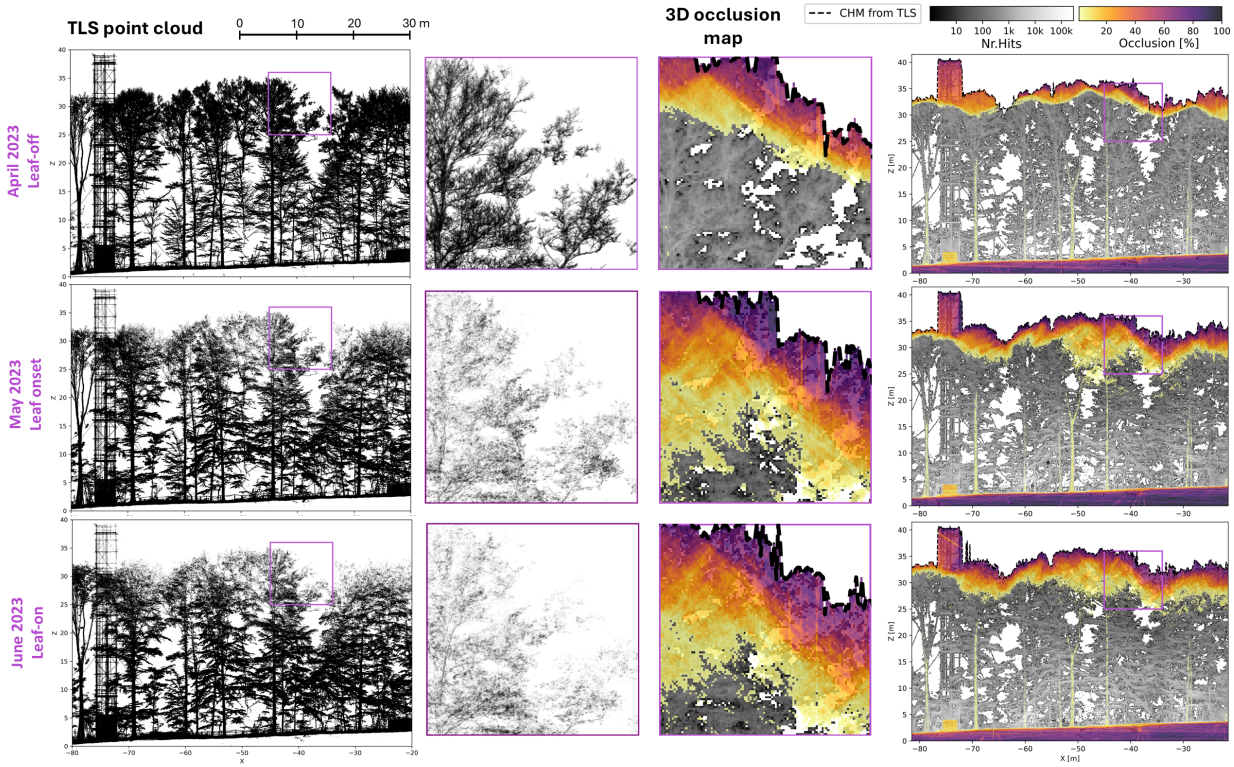

Figure 6: Illustration of the impact of leaves and forest structure on occlusion patterns using a multi-temporal terrestrial laser scanning (TLS) dataset from a temperate deciduous forest in Belgium, showing data from April (leaf-off), May (leaf onset) and June (leaf-on) on the top, middle and bottom, respectively. TLS point cloud data with zoom-in on an area in the top of the canopy (left) and their respective occlusion maps (right) show increased occlusion with leaf onset. Notably, occlusion can also be affected by the angles of the leaves and branches which change when more leaves appear and might reduce or increase occlusion in certain spots.

ing true changes from acquisition-related artefacts as effectively as possible. Quantifying occlusion provides critical insights into the representativeness of the point cloud and specific parts of it, enabling the rejection of apparent changes that arise from differing patterns of occluded space. This perspective becomes especially important when scanning conditions within the time series vary greatly, for example, when combining data from both leaf-on and leaf-off periods (Figure 6) or when incorporating datasets from different sensor types with their associated technical differences.

Occlusion mapping of multi-temporal laser scanning data can provide valuable insights into the differences in measurement uncertainty across time steps, which ideally should be incorporated into an overall uncertainty metric when quantifying change. This approach helps define the minimal amount of change or time difference required for changes to be reliably detected. Additionally, occlusion mapping can assist in determining the area of interest for analysis. For example, by mapping occlusion from leaf-off scans, we can identify the parts of the landscape that are theoretically scanable — that is, the full area the laser can reach without leaf interference. When analyzing summer scans of the same area, the analysis can then be restricted to these parts or adjusted to account for the occluded regions. Furthermore, differences in occlusion across multi-temporal datasets can also be used to explore the type of occlusion (geometric vs. full), since vegetation movement throughout the day can alter occlusion patterns.

5.5. Data prediction and point cloud completion

Various strategies have been developed not only to handle uncertainties in point cloud data but also to interpolate or reconstruct missing information arising from unobserved space during post-processing. Many of these approaches could benefit substantially from an explicit quantification of occlusion and unobserved space. Besides the previously mentioned approaches to compensate biases in vegetation density metrics, in the context of single tree reconstruction various methods have been proposed to infer structural information from incomplete point clouds. These approaches attempt to compensate for data gaps caused by occlusion, often by relying on morphological knowledge and growth patterns of trees. Approaches include algorithms that aim to reconstruct tubular shapes from noisy and occluded point clouds (Ravaglia et al., 2017) or cover the occluded regions of tree stems with an apriori model (Morel et al., 2018). Algorithms grounded in the topology of tree skeletons are also often employed to bridge gaps in the tree structure (Cao et al., 2022; Wang et al., 2023).

In general, 3D reconstruction algorithms aimed at approximating the surface or tree volume represented by the point cloud may benefit from distinguishing gaps caused by open space and gaps caused by occlusion, where assumptions about tree architecture must be made. The same goes for graph-based instance segmentation methods, where data gaps pose a major problem for segmenting individual trees from the forest. How these gaps are handled is data-dependent and often controlled by some user-set parameter, where

a balance must be struck between low values leading to oversegmentation and high values leading to undersegmentation, e.g. merging of smaller trees into one instance. Occlusion mapping may be useful in this application by providing a clear distinction between open space gaps, and gaps caused by occlusion.

Recent advances in deep learning have led to the development of point cloud completion networks that aim to reconstruct the full geometry of individual trees from partial observations (Xu et al., 2025; Zhang et al., 2025). These models are trained on large datasets of complete and partial tree point clouds (derived from real or simulated data) to learn structural priors and generate missing points. The completed point clouds can subsequently serve as input for a wide range of downstream analyses. For instance, Bornand et al. (2024) applied a deep learning-based point cloud completion approach to mitigate small scale gaps in dense point clouds of broadleaf trees. Partial and complete point clouds were derived from synthetic tree generation and laser scanning simulation and used to train the transformer-based PoinTr model. Results show the potential of deep learning for completion of partial point clouds. Integration of occlusion mapping results may further improve these models, by explicitly identifying the spatial regions requiring completion. This strategy is particularly useful when applied at the forest plot or stand level, where individual tree segmentation was not performed in advance. In such cases, occlusion mapping can be used to identify sparse regions of the point cloud, allowing the model to target only those areas and thereby

avoiding the computational burden and potential noise of processing the entire scene. A more advanced approach could even involve directly integrating occlusion mapping information into the model architecture itself.

Moreover, it remains an open question whether point cloud completion as a preprocessing step could potentially improve the performance of graph-based instance segmentation methods. Future research should investigate whether filling occluded regions leads to better-defined individual tree instances and more accurate segmentation results. An alternative to reconstructing complete point clouds would be to use state-of-the-art deep learning models to directly estimate target variables (such as above-ground biomass or vegetation density) from incomplete data. For such applications, it is essential to develop models that can tolerate missing information and incorporate occlusion bias. In this context, occlusion mapping would again serve as a critical component, providing models with a quantifiable measure of data incompleteness.

A key open challenge for all these data-driven approaches is transferability: completion and prediction networks learn structural priors specific to the species, growth forms and canopy architectures present in their training data, and a substantial domain gap exists in particular between synthetic training scenes and real-world acquisitions (Bornand et al., 2024). A model trained in one forest type or ecozone can therefore not be assumed to generalise to structurally distinct forests without retraining or fine-tuning on representative data. This places a premium on training data that span the

relevant structural diversity and that are themselves occlusion-aware, i.e. in which the occluded regions are known rather than inferred.

The success of any data-driven approach therefore depends fundamentally on the availability of large quantities of complete, representative training data. Assessing the completeness and quality of such data remains a major challenge. Currently, visual inspection is the most common method, but systematic occlusion mapping could provide a more robust and objective measure of training data quality in the future. A particular promising avenue for generating suitable training and validation datasets is the use of virtual laser scanning, discussed in the following subsection.

5.6. Virtual laser scanning to advance the study of occlusion

An inherent problem in occlusion mapping, and thereby also the development of evaluation tools and methods for compensation, is the lack of reference data on what space is occupied by vegetation and what space is empty. While complete coverage is impossible, the best approximation to the required reference data is very dense and high-resolution acquisitions from many viewpoints. Even these still suffer from their own occlusion effects and, since vegetation is not static, come with the challenge of time synchronisation. This makes it difficult to interpret occlusion mapping results in real-world data.

A potential solution to this problem is to simulate laser scanning in virtual vegetation scenes using tools like HELIOS++ or DART (Figure 7, Wini-

warter et al., 2022; Gastellu-Etchegorry et al., 2015; Abegg et al., 2023; Wei et al., 2020). We can thereby quantify exactly how much of the vegetation, not just how much of the overall space, is occluded and thus how much relevant information is missing. Virtual laser scanning (VLS) incorporates both necessary metadata for the occlusion mapping tools, such as sensor positions, and full knowledge about the component optical properties. As such, VLS can be used to compare and validate occlusion mapping algorithms and to investigate their sources of error. This includes intermediate technical steps such as assessing the accuracy of the reconstructed rays in the voxel traversal, since the true origins and vectors of each pulse are known.

VLS acts as a virtual playground for designing and evaluating survey strategies and allows systematic and controlled investigation of the different factors influencing occlusion, such as sensor specifications, acquisition settings, and forest structure (Figure 7, Section 3), which are provided as input to the simulations. This enables a better understanding of the magnitude and spatial location of occlusion effects and the effectiveness of approaches to compensation.

In the same way, the effect of occlusion on derived tree and stand-level metrics (see Table 4) can be quantified, since reference data for most of these metrics can be derived directly and automatically from the input VLS scene without error (Winiwarter et al., 2022), and metrics can be compared between VLS scenarios with and without occlusion (Yun et al., 2019). Virtual scenes can be parametrized to replicate real conditions, e.g., tree species,

tree height and diameter distributions, and stand densities, which means the effects of occlusion can be investigated for specific forest sites.

All the above analyses require that the simulation, which is always a simplified model of real-world conditions, is sufficiently realistic to effectively reproduce the underlying processes. Thus, while the results need to be confirmed with real experiments, insights from VLS-based sensitivity analyses may allow for informed and cost-effective optimisation of survey plans. Although extremely high-resolution reconstructions of forest scenes from TLS are possible in principle, their creation is highly demanding in terms of field effort and processing time (e.g. Zhu et al., 2023), and the degree of realism required to generate realistic levels of occlusion remains an open question.

Beyond occlusion analysis, VLS tools such as HELIOS++ and DART provide a bridge to radiative transfer modelling, since the same virtual forest scenes that are used to simulate laser scanning can simultaneously serve as input to radiative transfer simulations (see also Section 5.7). This coupling allows the effect of occlusion-induced structural gaps on canopy traits relevant for the radiative transfer, such as vegetation densities, to be studied in a fully controlled environment, where both the true structural reference and the occluded observations are known.

5.7. Radiative transfer and forest modelling

Forest structure regulates light availability within the canopy (Kükenbrink et al., 2021), influencing processes related to energy and matter fluxes (Damm

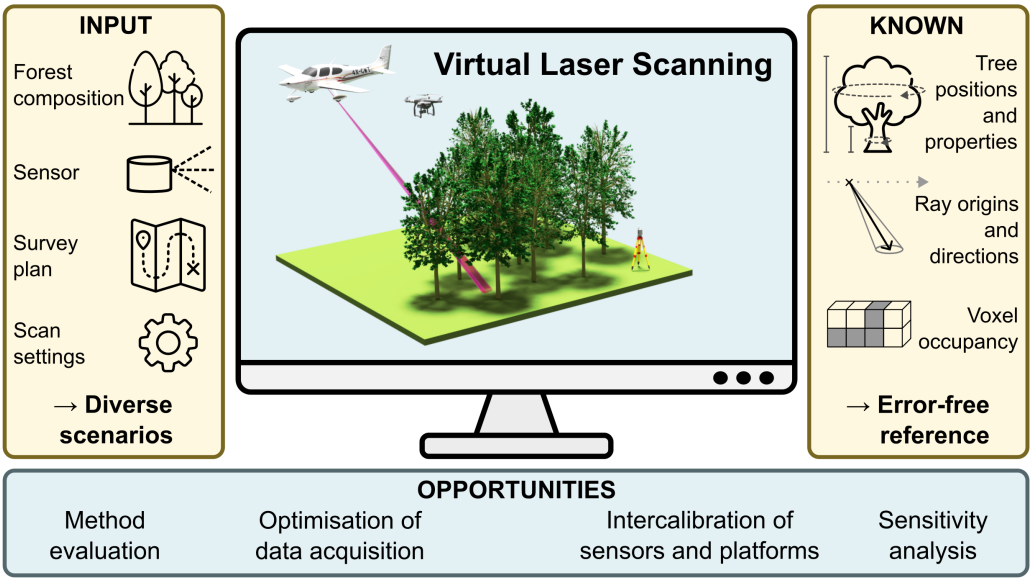

Figure 7: Demonstration of the opportunities from virtual laser scanning (VLS): The operator can vary the composition of the virtual forest, the sensor, the survey plan and the survey settings, enabling diverse and targeted acquisition scenarios (left panel). In the simulated environment, the tree properties, the origins and the directions of the virtual pulses and the occupancy of scene voxels are known and therefore provide error-free reference (right panel). This enables evaluating occlusion quantification methods, conducting sensitivity analyses, and optimising specific data acquisitions.

et al., 2020; Kesselring et al., 2024) and consequently shapes forest functioning and its future development. Radiative transfer and forest growth models seek to simulate this complex light-canopy interaction, with the goal to improve the understanding of forest function as well as the signal received with passive optical airborne and satellite sensors (e.g. Damm et al., 2020; Kesselring et al., 2024). These models heavily rely on an accurate representation of the complex 3D structure, which is often derived from laser scanning acquisitions (e.g. Schneider et al., 2014). Occlusion therefore directly influences the capacity to accurately model these complex light-canopy interactions. When portions of the canopy are systematically missed due to occlusion, radiative transfer models that rely on laser scanning derived structural inputs, such as LAD or PAD profiles (see Section 5.3), inherit those data gaps and may therefore produce biased estimates of light interception, canopy transmittance, or shortwave radiation absorption (e.g. Widlowski et al., 2015; Schneider et al., 2019b). Physically-based radiative transfer models such as DART (Gastellu-Etchegorry et al., 2015) and SCOPE (van der Tol et al., 2009) increasingly rely on point clouds or voxel grids to parameterise 3D vegetation scenes, but occluded voxels are typically left empty or filled with assumptions, propagating structural uncertainty into modelled fluxes. Therefore, incorporating occlusion maps into this workflow offers a direct way to flag unreliable input regions (see also Section 5.2), guide gap-filling strategies (see also Section 5.5 and Section 5.3), or weight structural observations according to their sampling confidence.

Looking further ahead, occlusion-aware terrestrial (TLS, MLS) and airborne (ALS, ULS) laser scanning plays an important role in the calibration and validation (cal/val) of current and upcoming satellite missions targeting vegetation structure and function, such as GEDI, ICESat2, BIOMASS, or FLEX (e.g. Duncanson et al., 2022; Drusch et al., 2017). While airborne and terrestrial laser scanning are increasingly used as reference for canopy height products, their use for validating PAD, LAI, or the fraction of absorbed photosynthetically active radiation (fAPAR) retrievals remains limited. This is in part because occlusion induced biases in these metrics are rarely quantified or reported alongside the reference data (see also Section 5.3 or Schneider et al., 2019a). As the good practice guidelines for cal/val of satellite-derived vegetation products of the Committee on Earth Observation Satellites (CEOS) continue to evolve, occlusion mapping could become a standard quality indicator accompanying laser-scanning derived reference datasets, enabling more transparent and robust validation of satellite biophysical products across diverse forest ecosystems.

6. Conclusion

In this perspective, we have argued that occlusion is best understood not only as a challenge to be minimised, but as a mappable and actionable property of forest laser scanning data. Occlusion is a major and pervasive effect that can heavily bias forest structure analysis and interpretation if left unexamined. Yet, by quantifying it explicitly, the same effect becomes an in-

formative measure of point cloud completeness and reliability. By providing a structured synthesis of the concept of occlusion, we set up the theoretical background for a better understanding of its causes, showing the influence of various factors (from forest structure to acquisition strategies, laser instrument properties and interlinked effects). Building upon this, we provided and discussed a range of cross-platform strategies for mitigating occlusion and presented best-practice guidelines for optimized laser scanning acquisitions for forest structure assessment. Our overview of different software tools demonstrated that practical implementations of occlusion mapping are already possible across different programming languages, marking an important step towards greater user accessibility in this field. We further raised awareness that selected metadata information to the point clouds, such as scan position and trajectory information, is essential for occlusion mapping and should therefore be provided and stored alongside the 3D data itself.

Although occlusion is recognized as a major challenge in laser scanning of forests and the retrieval of forest and tree structural parameters, it is rarely explicitly quantified or used as a quality metric of the acquired point clouds. Spatial mapping and quantification of occlusion open up a plethora of exciting research opportunities. These range from point cloud quality assessment and the quantification of uncertainties in point-cloud-derived forest metrics, to cutting-edge topics such as point cloud completion and virtual laser scanning. Looking further ahead, occlusion-aware reference data could also be integrated into radiative transfer modelling and the calibration and valida-

tion of satellite-derived vegetation products. We see that through occlusion mapping, new ways to acquire point clouds using adaptive, intelligent acquisition strategies to maximize canopy observation will emerge in the near future, further improving point cloud quality and accuracy of derived forest or tree metrics. We encourage researchers, practitioners, and technology developers to incorporate and advance occlusion-aware approaches, enabling a next generation of forest laser scanning. Given the increasing need to monitor forest structural changes in the face of global change, occlusion mapping may help ensuring robust and reliable extraction of structural information from multi-temporal laser scanning data. These advancements in assessing forest structural dynamics align with policy frameworks such as the European Union Biodiversity Strategy and the principles of close-to-nature forest management, which emphasize enhancing structural diversity to support forest resilience, long-term productivity, sustainable use, and biodiversity conservation.

CRediT author statement

Daniel Kükenbrink: Conceptualisation, Writing - Original Draft, Writing - Review, Editing, Software, Investigation, Visualization, Supervision & Project administration; **Matthias Gassilloud**: Conceptualisation, Writing - Original Draft, Writing - Review, Editing & Software; **Benjamin Brede**: Conceptualisation, Writing - Original Draft, Writing - Review, Editing, Software & Supervision; **Aline Bornand**: Writing - Review & Editing; **Kim**

Calders: Conceptualisation, Writing - Review & Editing; **Wout Cherlet**: Visualization, Writing - Review & Editing; **Markus P Eichhorn**: Writing - Review & Editing; **Julian Frey**: Writing - Review & Editing; **Charis Moana Gretler**: Visualization; **Bernhard Höfle**: Conceptualisation, Writing - Review & Editing; **Teja Kattenborn**: Conceptualisation, Writing - Review & Editing; **Lennart Klinger**: Software & Investigation; **Martin Mokroš**: Conceptualisation, Writing - Review & Editing; **Timo P Pitkänen**: Conceptualisation, Writing - Review & Editing; **Ninni Saarinen**: Conceptualisation, Writing - Review & Editing; **Louise Terryn**: Visualization, Writing - Review & Editing; **Hannah Weiser**: Conceptualisation, Visualization, Writing - Review & Editing; **Anna Göritz**: Conceptualisation, Writing - Original Draft, Writing - Review, Editing & Supervision;

Acknowledgements

This article/publication is based upon work from COST Action 3DForEcoTech, CA20118, supported by COST (European Cooperation in Science and Technology). D.K. was supported by the Swiss National Forest Inventory (NFI), a cooperative effort between the Swiss Federal Institute for Forest, Snow and Landscape Research (WSL) and the Swiss Federal Office for the Environment (FOEN). M.G. and A.G. would like to acknowledge funding by the Deutsche Forschungsgemeinschaft (DFG, German Research Foundation) - SFB 1537/1 (CRC ECOSENSE). B.B. acknowledges funding by the European Commission through NextGenCarbon project (grant

agreement 101184989). B.H. and H.W. were supported by the Deutsche Forschungsgemeinschaft (DFG, German Research Foundation) in the frame of the projects VirtuaLearn3D (project number: 496418931) and "Fostering a community-driven and sustainable HELIOS++ scientific software" (project number: 528521476). T.K. was supported by the Deutsche Forschungsgemeinschaft (DFG, German Research Foundation) in the frame of the projects LeafH2O (project number: 541018379). N.S. and T.P. were funded by the Research Council of Finland through the UNITE flagship (grant numbers 357906 & 357909). L.T. was funded by Ghent University (Ghent University Bijzonder Onderzoeksfonds Grant No. 01G01923). K.C. and W.C. were funded by the European Union (ERC-2021-STG Grant agreement No. 101039795). Views and opinions expressed are however those of the author(s) only and do not necessarily reflect those of the European Union or the European Research Council Executive Agency. Neither the European Union nor the granting authority can be held responsible for them. Figure 7 shows tree icons made by Freepik, a map icon made by Smashicons, settings icon made by Pixel perfect all available through `www.flaticon.com`. The central 3D scene in Figure 7 is rendered in Blender with an aeroplane model CC-BY Emmanuel Beranger and a drone model by cgtrader.com user `CGaxr`.

Declaration of Generative AI and AI-Assisted Technologies in the Writing Process

During the preparation of this work the author(s) used ChatGPT and Claude in order to improve the readability and language. After using this tool/service, the author(s) reviewed and edited the content as needed and take(s) full responsibility for the content of the published article.

References

Abegg, M., Boesch, R., Schaepman, M.E., Morsdorf, F., 2021. Impact of Beam Diameter and Scanning Approach on Point Cloud Quality of Terrestrial Laser Scanning in Forests. IEEE Transactions on Geoscience and Remote Sensing 59, 8153–8167. URL: https://ieeexplore.ieee.org/document/9286414/, doi:10.1109/TGRS.2020.3037763.

Abegg, M., Bösch, R., Kükenbrink, D., Morsdorf, F., 2023. Tree volume estimation with terrestrial laser scanning — testing for bias in a 3d virtual environment. Agricultural and Forest Meteorology 331, 109348. URL: https://www.sciencedirect.com/science/article/pii/S0168192323000424, doi:https://doi.org/10.1016/j.agrformet.2023.109348.

Abegg, M., Kükenbrink, D., Zell, J., Schaepman, M.E., Morsdorf, F., 2017. Terrestrial Laser Scanning for Forest Inventories—Tree Diameter Distribution and Scanner Location Impact on Occlusion. Forests 8, 184. doi:10.3390/f8060184.

Amanatides, J., Woo, A., 1987. A fast voxel traversal algorithm for ray tracing. Proceedings of EUROGRAPHICS 87, 3–10. URL: http://www.cse.yorku.ca/~amana/research/grid.pdf. paper describing the algorithm used for ray tracing!

Bai, Y., Verley, P., Yin, T., Lauret, N., Forbes, F., Durand, J.B., Vincent, G., 2026. Pulse fragmentation-induced uncertainty in forest LAI mapping using UAV LiDAR. Remote Sensing of Environment 338, 115341. doi:10.1016/j.rse.2026.115341.

Barrere, J., Reineking, B., Jaunatre, M., Kunstler, G., 2024. Forest storm resilience depends on the interplay between functional composition and climate—Insights from European-scale simulations. Functional Ecology 38, 500–516. doi:10.1111/1365-2435.14489.

Bartholomeus, H., Calders, K., Whiteside, T., Terryn, L., Krishna Moorthy, S.M., Levick, S.R., Bartolo, R., Verbeeck, H., 2022. Evaluating Data Inter-Operability of Multiple UAV–LiDAR Systems for Measuring the 3D Structure of Savanna Woodland. Remote Sensing 14, 5992. doi:10.3390/rs14235992.

Béland, M., Kobayashi, H., 2021. Mapping forest leaf area density from multiview terrestrial lidar. Methods in Ecology and Evolution 12, 619–633. doi:10.1111/2041-210X.13550.

Bienert, A., Queck, R., Schmidt, A., Bernhofer, C., 2010. VOXEL SPACE

ANALYSIS OF TERRESTRIAL LASER SCANS IN FORESTS FOR WIND FIELD MODELING. International Archives of Photogrammetry. Remote Sensing and Spatial Information Sciences 38, 92–97.

Bornand, A., Abegg, M., Morsdorf, F., Rehush, N., 2024. Completing 3D point clouds of individual trees using deep learning. Methods in Ecology and Evolution 2024, 1–14. doi:10.1111/2041-210X.14412.

Boucher, P.B., Paynter, I., Orwig, D.A., Valencius, I., Schaaf, C., 2021. Sampling forests with terrestrial laser scanning. Annals of Botany 128, 689–708. doi:10.1093/aob/mcab073.

Breda, N.J.J., 2003. Ground-based measurements of leaf area index: A review of methods, instruments and current controversies. Journal of Experimental Botany 54, 2403–2417. doi:10.1093/jxb/erg263.

Brede, B., Bartholomeus, H.M., Barbier, N., Pimont, F., Vincent, G., Herold, M., 2022. Peering through the thicket: Effects of UAV LiDAR scanner settings and flight planning on canopy volume discovery. International Journal of Applied Earth Observation and Geoinformation 114, 103056. URL: https://doi.org/10.1016/j.jag.2022.103056, doi:10.1016/j.jag.2022.103056.

Brede, B., Kükenbrink, D., Höfle, B., Kattenborn, T., Klinger, L., Pitkänen, T., Singh, A., Weiser, H., 2023. Occlusion mapping tools for point cloud

quality assessment in forest laser scanning, in: SilviLaser 2023, London (UK).

Brede, B., Lau, A., Bartholomeus, H., Kooistra, L., 2017. Comparing RIEGL RiCOPTER UAV LiDAR derived canopy height and DBH with terrestrial LiDAR. Sensors 17, 2371. URL: https://www.mdpi.com/1424-8220/17/10/2371, doi:10.3390/s17102371.

Brede, B., Pimont, F., Vincent, G., Schiedewitz, O., 2025. voxelizer: advanced functionalities for voxelizing lidar point cloud data. URL: https://doi.org/10.5281/zenodo.16759585.

Béland, M., Baldocchi, D.D., Widlowski, J.L., Fournier, R.A., Verstraete, M.M., 2014. On seeing the wood from the leaves and the role of voxel size in determining leaf area distribution of forests with terrestrial LiDAR. Agricultural and Forest Meteorology 184, 82–97. URL: https://linkinghub.elsevier.com/retrieve/pii/S0168192313002608, doi:10.1016/j.agrformet.2013.09.005.

Béland, M., Widlowski, J.L., Fournier, R.A., Côté, J.F., Verstraete, M.M., 2011. Estimating leaf area distribution in savanna trees from terrestrial LiDAR measurements. Agricultural and Forest Meteorology 151, 1252–1266. URL: https://linkinghub.elsevier.com/retrieve/pii/S0168192311001481, doi:10.1016/j.agrformet.2011.05.004.

Calders, K., Adams, J., Armston, J., Bartholomeus, H., Bauwens, S., Bent-

ley, L.P., Chave, J., Danson, F.M., Demol, M., Disney, M., Gaulton, R., Krishna Moorthy, S.M., Levick, S.R., Saarinen, N., Schaaf, C., Stovall, A., Terryn, L., Wilkes, P., Verbeeck, H., 2020. Terrestrial laser scanning in forest ecology: Expanding the horizon. Remote Sensing of Environment 251, 112102. URL: https://linkinghub.elsevier.com/retrieve/pii/S0034425720304752, doi:10.1016/j.rse.2020.112102.

Calders, K., Armston, J., Newnham, G., Herold, M., Goodwin, N., 2014. Implications of sensor configuration and topography on vertical plant profiles derived from terrestrial LiDAR. Agricultural and Forest Meteorology 194, 104–117. doi:10.1016/j.agrformet.2014.03.022.

Calders, K., Herold, M., Adams, J., Armston, J., Brede, B., Cherlet, W., Cooper, Z.T., Dayal, K., Frenne, P.D., Levick, S.R., Meir, P., Origo, N., Senf, C., Soenens, L., Terryn, L., Van Den Broeck, W.A., Vastaranta, M., Verbeeck, H., Villard, L., Disney, M., 2025. Realistic virtual forests for understanding forest disturbances and recovery from space. ISPRS Journal of Photogrammetry and Remote Sensing 227, 501–507. doi:10.1016/j.isprsjprs.2025.06.031.

Calders, K., Origo, N., Disney, M., Nightingale, J., Woodgate, W., Armston, J., Lewis, P., 2018. Variability and bias in active and passive ground-based measurements of effective plant, wood and leaf area index. Agricultural and Forest Meteorology 252, 231–240. doi:10.1016/j.agrformet.2018.01.029.

Cao, W., Wu, J., Shi, Y., Chen, D., 2022. Restoration of individual tree missing point cloud based on local features of point cloud. Remote Sensing 14. URL: https://doi.org/10.3390/rs14061346, doi:10.3390/rs14061346. number: 6.

Chirici, G., Giannetti, F., D'Amico, G., Vangi, E., Francini, S., Borghi, C., Corona, P., Travaglini, D., 2023. Robotics in forest inventories: Spot's first steps. Forests 14. URL: https://www.mdpi.com/1999-4907/14/11/2170, doi:10.3390/f14112170.

Chisholm, R., Cui, J., Lum, S., Chen, B.M., 2013. UAV LiDAR for below-canopy forest surveys. Journal of Unmanned Vehicle Systems doi:dx.doi.org/10.1139/juvs-2013-0017.

Computree Core Team, 2024. Computree platform. Computree group. URL: https://computree.onf.fr.

Côté, J.F., Fournier, R.A., Egli, R., 2011. An architectural model of trees to estimate forest structural attributes using terrestrial LiDAR. Environmental Modelling & Software 26, 761–777. doi:10.1016/j.envsoft.2010.12.008.

Dalla Corte, A.P., de Vasconcellos, B.N., Rex, F.E., Sanquetta, C.R., Mohan, M., Silva, C.A., Klauberg, C., de Almeida, D.R.A., Zambrano, A.M.A., Trautenmüller, J.W., Leite, R.V., do Amaral, C.H., Veras, H.F.P., da Silva Rocha, K., de Moraes, A., Karasinski, M.A., Sanquetta, M.N.I.,

Broadbent, E.N., 2022. Applying High-Resolution UAV-LiDAR and Quantitative Structure Modelling for Estimating Tree Attributes in a Crop-Livestock-Forest System. Land 11, 507. URL: https://www.mdpi.com/2073-445X/11/4/507, doi:10.3390/land11040507.

Damm, A., Paul-Limoges, E., Kükenbrink, D., Bachofen, C., Morsdorf, F., 2020. Remote sensing of forest gas exchange: Considerations derived from a tomographic perspective. Global Change Biology 26. doi:10.1111/gcb.15007.

Danson, F.M., Hetherington, D., Morsdorf, F., Koetz, B., Allgower, B., 2007. Forest Canopy Gap Fraction From Terrestrial Laser Scanning. IEEE Geoscience and Remote Sensing Letters 4, 157–160. doi:10.1109/LGRS.2006.887064.

Davison, S., Donoghue, D.N., Galiatsatos, N., 2020. The effect of leaf-on and leaf-off forest canopy conditions on LiDAR derived estimations of forest structural diversity. International Journal of Applied Earth Observation and Geoinformation 92, 102160. URL: https://linkinghub.elsevier.com/retrieve/pii/S0303243420300684, doi:10.1016/j.jag.2020.102160.

D'hont, B., Calders, K., Antonelli, A., Berg, T., Cherlet, W., Dayal, K., Fitzpatrick, O.J., Hambrecht, L., Leponce, M., Lucieer, A., Pascal, O., Raumonen, P., Verbeeck, H., 2025. Integrating terrestrial and canopy

laser scanning for comprehensive analysis of large old trees: Implications for single tree and biodiversity research. Remote Sensing in Ecology and Conservation n/a. doi:10.1002/rse2.70021.

Disney, M., 2021. How can we know what we don't know? A Commentary on: Sampling forests with terrestrial laser scanning. Annals of Botany 128, 685–688. doi:10.1093/aob/mcab119.

Disney, M., Kalogirou, V., Lewis, P., Prieto-Blanco, A., Hancock, S., Pfeifer, M., 2010. Simulating the impact of discrete-return lidar system and survey characteristics over young conifer and broadleaf forests. Remote Sensing of Environment 114, 1546–1560. URL: https://linkinghub.elsevier.com/retrieve/pii/S0034425710000684, doi:10.1016/j.rse.2010.02.009.

Drusch, M., Moreno, J., Del Bello, U., Franco, R., Goulas, Y., Huth, A., Kraft, S., Middleton, E.M., Miglietta, F., Mohammed, G., Nedbal, L., Rascher, U., Schüttemeyer, D., Verhoef, W., 2017. The FLuorescence EXplorer Mission Concept—ESA's Earth Explorer 8. IEEE Transactions on Geoscience and Remote Sensing 55, 1273–1284. doi:10.1109/TGRS.2016.2621820.

Duncanson, L., Kellner, J.R., Armston, J., Dubayah, R., Minor, D.M., Hancock, S., Healey, S.P., Patterson, P.L., Saarela, S., Marselis, S., Silva, C.E., Bruening, J., Goetz, S.J., Tang, H., Hofton, M., Blair, B., Luthcke,

S., Fatoyinbo, L., Abernethy, K., Alonso, A., Andersen, H.E., Aplin, P., Baker, T.R., Barbier, N., Bastin, J.F., Biber, P., Boeckx, P., Bogaert, J., Boschetti, L., Boucher, P.B., Boyd, D.S., Burslem, D.F., Calvo-Rodriguez, S., Chave, J., Chazdon, R.L., Clark, D.B., Clark, D.A., Cohen, W.B., Coomes, D.A., Corona, P., Cushman, K., Cutler, M.E., Dalling, J.W., Dalponte, M., Dash, J., de-Miguel, S., Deng, S., Ellis, P.W., Erasmus, B., Fekety, P.A., Fernandez-Landa, A., Ferraz, A., Fischer, R., Fisher, A.G., García-Abril, A., Gobakken, T., Hacker, J.M., Heurich, M., Hill, R.A., Hopkinson, C., Huang, H., Hubbell, S.P., Hudak, A.T., Huth, A., Imbach, B., Jeffery, K.J., Katoh, M., Kearsley, E., Kenfack, D., Kljun, N., Knapp, N., Král, K., Krůček, M., Labrière, N., Lewis, S.L., Longo, M., Lucas, R.M., Main, R., Manzanera, J.A., Martínez, R.V., Mathieu, R., Memiaghe, H., Meyer, V., Mendoza, A.M., Monerris, A., Montesano, P., Morsdorf, F., Næsset, E., Naidoo, L., Nilus, R., O'Brien, M., Orwig, D.A., Papathanassiou, K., Parker, G., Philipson, C., Phillips, O.L., Pisek, J., Poulsen, J.R., Pretzsch, H., Rüdiger, C., Saatchi, S., Sanchez-Azofeifa, A., Sanchez-Lopez, N., Scholes, R., Silva, C.A., Simard, M., Skidmore, A., Stereńczak, K., Tanase, M., Torresan, C., Valbuena, R., Verbeeck, H., Vrska, T., Wessels, K., White, J.C., White, L.J., Zahabu, E., Zgraggen, C., 2022. Aboveground biomass density models for NASA's Global Ecosystem Dynamics Investigation (GEDI) lidar mission. Remote Sensing of Environment 270, 112845. doi:10.1016/j.rse.2021.112845.

Ehbrecht, M., Schall, P., Juchheim, J., Ammer, C., Seidel, D., 2026. Effective

number of layers: A new measure for quantifying three-dimensional stand structure based on sampling with terrestrial LiDAR. Forest Ecology and Management 380, 212–223. URL: http://linkinghub.elsevier.com/retrieve/pii/S0378112716305102, doi:10.1016/j.foreco.2016.09.003.

Ehbrecht, M., Seidel, D., Annighöfer, P., Kreft, H., Köhler, M., Zemp, D.C., Puettmann, K., Nilus, R., Babweteera, F., Willim, K., Stiers, M., Soto, D., Boehmer, H.J., Fisichelli, N., Burnett, M., Juday, G., Stephens, S.L., Ammer, C., 2021. Global patterns and climatic controls of forest structural complexity. Nature Communications 12, 519. doi:10.1038/s41467-020-20767-z.

Eisoldt, M., Mock, A., Wiemann, T., Porrmann, M., 2025. Efficient global 6d localization in 3d tsdf maps using point-wise and scan-wise reduction methods on embedded gpus. International Journal of Semantic Computing 0, null. URL: https://doi.org/10.1142/S1793351X25410053, doi:10.1142/S1793351X25410053, arXiv:https://doi.org/10.1142/S1793351X25410053.

Freißmuth, L., Mattamala, M., Chebrolu, N., Schaefer, S., Leutenegger, S., Fallon, M., 2024. Online tree reconstruction and forest inventory on a mobile robotic system, in: 2024 IEEE/RSJ International Conference on Intelligent Robots and Systems (IROS), pp. 11765–11772. doi:10.1109/IROS58592.2024.10802455.

Frey, J., Schindler, Z., McClatchy, P., Morhart, C., Larysch, E., Seifert,

T., 2025. The 3d reconstruction of wood and leaves from terrestrial laser scanning – a case study on PAR measurements below a solitary malus domestica tree. Silva Fennica 59. URL: https://www.silvafennica.fi/article/24027, doi:10.14214/sf.24027.

Gassilloud, M., Koch, B., Göritz, A., 2025. Occlusion mapping reveals the impact of flight and sensing parameters on vertical forest structure exploration with cost-effective uav based laser scanning. International Journal of Applied Earth Observation and Geoinformation 139, 104493.

Gastellu-Etchegorry, J.P., Yin, T., Lauret, N., Cajgfinger, T., Gregoire, T., Grau, E., Feret, J.B., Lopes, M., Guilleux, J., Dedieu, G., Malenovský, Z., Cook, B.D., Morton, D., Rubio, J., Durrieu, S., Cazanave, G., Martin, E., Ristorcelli, T., 2015. Discrete Anisotropic Radiative Transfer (DART 5) for Modeling Airborne and Satellite Spectroradiometer and LIDAR Acquisitions of Natural and Urban Landscapes. Remote Sensing 7, 1667–1701. doi:10.3390/rs70201667.

Gollob, C., Ritter, T., Nothdurft, A., 2020. Forest inventory with long range and high-speed personal laser scanning (PLS) and simultaneous localization and mapping (SLAM) technology. Remote Sensing 12. doi:10.3390/RS12091509.

Hancock, S., Armston, J., Li, Z., Gaulton, R., Lewis, P., Disney, M., Mark Danson, F., Strahler, A., Schaaf, C., Anderson, K., Gaston, K.J.,

2015. Waveform lidar over vegetation: An evaluation of inversion methods for estimating return energy. Remote Sensing of Environment 164, 208–224. URL: https://linkinghub.elsevier.com/retrieve/pii/S003442571500142X, doi:10.1016/j.rse.2015.04.013.

Hartley, R.J.L., Jayathunga, S., Morgenroth, J., Pearse, G.D., 2024. Tree branch characterisation from point clouds: a comprehensive review. Current Forestry Reports 10, 360–385. URL: https://link.springer.com/10.1007/s40725-024-00225-5, doi:10.1007/s40725-024-00225-5.

Heidrich, L., Bae, S., Levick, S., Seibold, S., Weisser, W., Krzystek, P., Magdon, P., Nauss, T., Schall, P., Serebryanyk, A., Wöllauer, S., Ammer, C., Bässler, C., Doerfler, I., Fischer, M., Gossner, M.M., Heurich, M., Hothorn, T., Jung, K., Kreft, H., Schulze, E.D., Simons, N., Thorn, S., Müller, J., 2020. Heterogeneity–diversity relationships differ between and within trophic levels in temperate forests. Nature Ecology & Evolution 4, 1204–1212. URL: https://www.nature.com/articles/s41559-020-1245-z, doi:10.1038/s41559-020-1245-z. bandiera_abtest: a Cg_type: Nature Research Journals Number: 9 Primary_atype: Research Publisher: Nature Publishing Group Subject_term: Community ecology;Forest ecology;Forestry;Theoretical ecology Subject_term_id: community-ecology;forest-ecology;forestry;theoretical-ecology.

Heidrich, L., Brandl, R., Ammer, C., Bae, S., Bässler, C., Doerfler, I., Fischer, M., Gossner, M.M., Heurich, M., Heibl, C., Jung, K., Krzystek,

P., Levick, S., Magdon, P., Schall, P., Schulze, E.D., Seibold, S., Simons, N.K., Thorn, S., Weisser, W.W., Wöllauer, S., Müller, J., 2023. Effects of heterogeneity on the ecological diversity and redundancy of forest fauna. Basic and Applied Ecology 73, 72–79. URL: https://linkinghub.elsevier.com/retrieve/pii/S1439179123000610, doi:10.1016/j.baae.2023.10.005.

Helbach, J., Frey, J., Messier, C., Mörsdorf, M., Scherer-Lorenzen, M., 2022. Light heterogeneity affects understory plant species richness in temperate forests supporting the heterogeneity–diversity hypothesis. Ecology and Evolution 12, e8534. URL: https://onlinelibrary.wiley.com/doi/abs/10.1002/ece3.8534, doi:10.1002/ece3.8534. _eprint: https://onlinelibrary.wiley.com/doi/pdf/10.1002/ece3.8534.

Hopkinson, C., 2007. The influence of flying altitude, beam divergence, and pulse repetition frequency on laser pulse return intensity and canopy frequency distribution. Canadian Journal of Remote Sensing 33, 312–324. doi:10.5589/m07-029.

Hopkinson, C., Chasmer, L., 2009. Testing LiDAR models of fractional cover across multiple forest ecozones. Remote Sensing of Environment 113, 275–288. doi:10.1016/j.rse.2008.09.012.

Huertas, C., Sabatier, D., Derroire, G., Ferry, B., Jackson, T., Pélissier, R., Vincent, G., 2022. Mapping tree mortality rate in a tropical moist

forest using multi-temporal lidar. International Journal of Applied Earth Observation and Geoinformation 109, 102780. URL: https://www.sciencedirect.com/science/article/pii/S0303243422001064, doi:https://doi.org/10.1016/j.jag.2022.102780.

Hyyppä, E., Hyyppä, J., Hakala, T., Kukko, A., Wulder, M.A., White, J.C., Pyörälä, J., Yu, X., Wang, Y., Virtanen, J.P., Pohjavirta, O., Liang, X., Holopainen, M., Kaartinen, H., 2020. Under-canopy UAV laser scanning for accurate forest field measurements. ISPRS Journal of Photogrammetry and Remote Sensing 164, 41–60. doi:10.1016/j.isprsjprs.2020.03.021.

Jactel, H., Bauhus, J., Boberg, J., Bonal, D., Castagneyrol, B., Gardiner, B., Gonzalez-Olabarria, J.R., Koricheva, J., Meurisse, N., Brockerhoff, E.G., 2017. Tree Diversity Drives Forest Stand Resistance to Natural Disturbances. Current Forestry Reports 3, 223–243. doi:10.1007/s40725-017-0064-1.

Jung, J., Pekin, B.K., Pijanowski, B.C., 2013. Mapping open space in an old-growth, secondary-growth, and selectively-logged tropical rainforest using discrete return LIDAR. IEEE Journal of Selected Topics in Applied Earth Observations and Remote Sensing 6, 2453–2461. URL: http://ieeexplore.ieee.org/document/6494343/, doi:10.1109/JSTARS.2013.2253306.

Karjalainen, V., Koivumäki, N., Hakala, T., Muhojoki, J., Hyyppä, E., George, A., Suomalainen, J., Honkavaara, E., 2025. Towards autonomous

photogrammetric forest inventory using a lightweight under-canopy robotic drone. URL: https://arxiv.org/abs/2501.12073, arXiv:2501.12073.

Kesselring, J., Morsdorf, F., Kükenbrink, D., Gastellu-Etchegorry, J.P., Damm, A., 2024. Diversity of 3D APAR and LAI dynamics in broadleaf and coniferous forests: Implications for the interpretation of remote sensing-based products. Remote Sensing of Environment 306, 114116. doi:10.1016/j.rse.2024.114116.

Knuff, A.K., Staab, M., Frey, J., Dormann, C.F., Asbeck, T., Klein, A.M., 2020. Insect abundance in managed forests benefits from multi-layered vegetation. Basic and Applied Ecology 48, 124–135. URL: http://www.sciencedirect.com/science/article/pii/S143917912030092X, doi:10.1016/j.baae.2020.09.002.

Kükenbrink, D., Marty, M., Rehush, N., Abegg, M., Ginzler, C., 2025. Evaluating the potential of handheld mobile laser scanning for an operational inclusion in a national forest inventory – A Swiss case study. Remote Sensing of Environment 321, 114685. doi:10.1016/j.rse.2025.114685.

Kükenbrink, D., Schneider, F., Leiterer, R., Schaepman, M., Morsdorf, F., 2017. Quantification of hidden canopy volume of airborne laser scanning data using a voxel traversal algorithm. Remote Sensing of Environment 194. doi:10.1016/j.rse.2016.10.023.

Kükenbrink, D., Schneider, F.D., Schmid, B., Gastellu-Etchegorry, J.P.,

Schaepman, M.E., Morsdorf, F., 2021. Modelling of three-dimensional, diurnal light extinction in two contrasting forests. Agricultural and Forest Meteorology 296, 108230. URL: https://doi.org/10.1016/j.agrformet.2020.108230https://linkinghub.elsevier.com/retrieve/pii/S0168192320303324, doi:10.1016/j.agrformet.2020.108230.

Lefsky, M.A., Cohen, W.B., Parker, G.G., Harding, D.J., 2002. Lidar Remote Sensing for Ecosystem Studies: Lidar, an emerging remote sensing technology that directly measures the three-dimensional distribution of plant canopies, can accurately estimate vegetation structural attributes and should be of particular interest to forest, landscape, and global ecologists. BioScience 52, 19–30. doi:10.1641/0006-3568(2002)052[0019:LRSFES]2.0.CO;2.

Li, L., Mu, X., Soma, M., Wan, P., Qi, J., Hu, R., 2020. An Iterative-Mode Scan Design of Terrestrial Laser Scanning in Forests for Minimizing Occlusion Effects. IEEE Transactions on Geoscience and Remote Sensing 59, 3547–3566. doi:10.1109/TGRS.2020.3018643.

Liang, X., Kukko, A., Balenović, I., Saarinen, N., Junttila, S., Kankare, V., Holopainen, M., Mokroš, M., Surový, P., Kaartinen, H., Jurjević, L., Honkavaara, E., Näsi, R., Liu, J., Hollaus, M., Tian, J., Yu, X., Pan, J., Cai, S., Virtanen, J.P., Wang, Y., Hyyppä, J., 2022. Close-range remote sensing of forests: The state of the art, challenges, and opportunities

for systems and data acquisitions. IEEE Geoscience and Remote Sensing Magazine 10, 32–71. doi:10.1109/MGRS.2022.3168135.

Liang, X., Liu, G., Dou, X., 2025. Under-canopy UAV Solutions for Forest Inventory – Challenges and Opportunities. The International Archives of the Photogrammetry, Remote Sensing and Spatial Information Sciences XLVIII-2-W11-2025, 183–188. doi:10.5194/isprs-archives-XLVIII-2-W11-2025-183-2025.

Loh, H.Y., James, D., Ioki, K., Wong, W.V.C., Tsuyuki, S., Phua, M.H., 2022. Estimating aboveground biomass changes in a human-modified tropical montane forest of borneo using multi-temporal airborne lidar data. Remote Sensing Applications: Society and Environment 28, 100821. doi:https://doi.org/10.1016/j.rsase.2022.100821.

Mathes, T., Seidel, D., Häberle, K.H., Pretzsch, H., Annighöfer, P., 2023. What Are We Missing? Occlusion in Laser Scanning Point Clouds and Its Impact on the Detection of Single-Tree Morphologies and Stand Structural Variables. Remote Sensing 15, 450. URL: https://www.mdpi.com/2072-4292/15/2/450, doi:10.3390/rs15020450.

Mattamala, M., Chebrolu, N., Casseau, B., Freißmuth, L., Frey, J., Tuna, T., Hutter, M., Fallon, M., 2024. Autonomous forest inventory with legged robots: System design and field deployment. URL: https://arxiv.org/abs/2404.14157, arXiv:2404.14157.

McRoberts, R.E., Næsset, E., Gobakken, T., Bollandsås, O.M., 2015. Indirect and direct estimation of forest biomass change using forest inventory and airborne laser scanning data. Remote Sensing of Environment 164, 36–42. URL: https://www.sciencedirect.com/science/article/pii/S0034425715000772, doi:https://doi.org/10.1016/j.rse.2015.02.018.

Milenković, M., Wagner, W., Quast, R., Hollaus, M., Ressl, C., Pfeifer, N., 2017. Total canopy transmittance estimated from small-footprint, full-waveform airborne LiDAR. ISPRS Journal of Photogrammetry and Remote Sensing 128, 61–72. doi:10.1016/j.isprsjprs.2017.03.008.

Mokroš, M., Mikita, T., Singh, A., Tomaštík, J., Chudá, J., Wezyk, P., Kuželka, K., Surový, P., Klimánek, M., Zieba-Kulawik, K., Bobrowski, R., Liang, X., 2021. Novel low-cost mobile mapping systems for forest inventories as terrestrial laser scanning alternatives. International Journal of Applied Earth Observation and Geoinformation 104, 102512. doi:10.1016/j.jag.2021.102512.

Morel, J., Bac, A., Véga, C., 2018. Surface reconstruction of incomplete datasets: A novel poisson surface approach based on CSRBF. Computers and Graphics (Pergamon) 74, 44–55. doi:10.1016/j.cag.2018.05.004. publisher: Pergamon.

Morhart, C., Schindler, Z., Frey, J., Sheppard, J.P., Calders, K., Disney, M., Morsdorf, F., Raumonen, P., Seifert, T., 2024. Limitations of estimating

branch volume from terrestrial laser scanning. European Journal of Forest Research 143, 687–702. doi:10.1007/s10342-023-01651-z.

Morsdorf, F., Frey, O., Meier, E., Itten, K.I., Allgöwer, B., 2008. Assessment of the influence of flying altitude and scan angle on biophysical vegetation products derived from airborne laser scanning. International Journal of Remote Sensing 29, 1387–1406. doi:10.1080/01431160701736349.

Morsdorf, F., Kötz, B., Meier, E., Itten, K., Allgöwer, B., 2006. Estimation of LAI and fractional cover from small footprint airborne laser scanning data based on gap fraction. Remote Sensing of Environment 104, 50–61. doi:10.1016/j.rse.2006.04.019.

Morsdorf, F., Kükenbrink, D., Schneider, F.D., Abegg, M., Schaepman, M.E., 2018. Close-range laser scanning in forests: Towards physically based semantics across scales. Interface Focus 8, 20170046. doi:10.1098/rsfs.2017.0046.

Morsdorf, F., Marty, M., Kükenbrink, D., 2025. UAV-based LiDAR and SfM-derived 3D point clouds of forest canopies - observation angles matter. Dreiländertagung D-A-CH 2025 "Raumbezogene Bilddaten und Künstliche Intelligenz für nachhaltige Lebensräume" , 338–350doi:10.24407/KXP:1928725848.

Moudrý, V., Cord, A.F., Gábor, L., Laurin, G.V., Barták, V., Gdulová, K., Malavasi, M., Rocchini, D., Stereńczak, K., Prošek, J., Klápště, P.,

Wild, J., 2023. Vegetation structure derived from airborne laser scanning to assess species distribution and habitat suitability: The way forward. Diversity and Distributions 29, 39–50. doi:10.1111/ddi.13644.

Næsset, E., 2009. Effects of different sensors, flying altitudes, and pulse repetition frequencies on forest canopy metrics and biophysical stand properties derived from small-footprint airborne laser data. Remote Sensing of Environment 113, 148–159. doi:10.1016/j.rse.2008.09.001.

Neuville, R., Bates, J.S., Jonard, F., 2021. Estimating Forest Structure from UAV-Mounted LiDAR Point Cloud Using Machine Learning. Remote Sensing 13, 352. URL: https://www.mdpi.com/2072-4292/13/3/352, doi:10.3390/rs13030352.

Nguyen, V.T., Fournier, R.A., Côté, J.F., Pimont, F., 2022. Estimation of vertical plant area density from single return terrestrial laser scanning point clouds acquired in forest environments. Remote Sensing of Environment 279, 113115. doi:10.1016/j.rse.2022.113115.

Pan, Y., Birdsey, R.A., Phillips, O.L., Jackson, R.B., 2013. The Structure, Distribution, and Biomass of the World's Forests. Annual Review of Ecology, Evolution, and Systematics 44, 593–622. doi:10.1146/annurev-ecolsys-110512-135914.

Panagiotidis, D., Abdollahnejad, A., Slavík, M., 2022. 3d point cloud fusion from UAV and TLS to assess temperate managed forest structures. Inter-

national Journal of Applied Earth Observation and Geoinformation 112, 102917. URL: https://linkinghub.elsevier.com/retrieve/pii/S1569843222001182, doi:10.1016/j.jag.2022.102917.

Pimont, F., Allard, D., Soma, M., Dupuy, J.L., 2018. Estimators and confidence intervals for plant area density at voxel scale with T-LiDAR. Remote Sensing of Environment 215, 343–370. doi:10.1016/j.rse.2018.06.024.

Pörtner, H.O., Scholes, R.J., Agard, J., Archer, E., Arneth, A., Bai, X., Barnes, D., Burrows, M., Chan, L., Cheung, W.L.W., Diamond, S., Donatti, C., Duarte, C., Eisenhauer, N., Foden, W., Gasalla, M.A., Handa, C., Hickler, T., Hoegh-Guldberg, O., Ichii, K., Jacob, U., Insarov, G., Kiessling, W., Leadley, P., Leemans, R., Levin, L., Lim, M., Maharaj, S., Managi, S., Marquet, P.A., McElwee, P., Midgley, G., Oberdorff, T., Obura, D., Osman Elasha, B., Pandit, R., Pascual, U., Pires, A.P.F., Popp, A., Reyes-García, V., Sankaran, M., Settele, J., Shin, Y.J., Sintayehu, D.W., Smith, P., Steiner, N., Strassburg, B., Sukumar, R., Trisos, C., Val, A.L., Wu, J., Aldrian, E., Parmesan, C., Pichs-Madruga, R., Roberts, D.C., Rogers, A.D., Díaz, S., Fischer, M., Hashimoto, S., Lavorel, S., Wu, N., Ngo, H., 2021. Scientific Outcome of the IPBES-IPCC Co-Sponsored Workshop on Biodiversity and Climate Change. Technical Report. Zenodo. doi:10.5281/ZENODO.4659158.

Prendes, C., Cabo, C., Ordoñez, C., Majada, J., Canga, E., 2021. An algorithm for the automatic parametrization of wood volume equations

from terrestrial laser scanning point clouds: application in *Pinus pinaster*. GIScience & Remote Sensing 58, 1130–1150. URL: https://www.tandfonline.com/doi/full/10.1080/15481603.2021.1972712, doi:10.1080/15481603.2021.1972712.

Qi, Z., Li, S., Pang, Y., Du, L., Zhang, H., Li, Z., 2023. Monitoring spatiotemporal variation of individual tree biomass using multitemporal lidar data. Remote Sensing 15. doi:10.3390/rs15194768.

Ravaglia, J., Bac, A., Fournier, R.A., 2017. Extraction of tubular shapes from dense point clouds and application to tree reconstruction from laser scanned data. Computers & Graphics 66, 23–33. doi:10.1016/J.CAG.2017.05.016. publisher: Pergamon.

Roussel, J.R., Caspersen, J., Béland, M., Thomas, S., Achim, A., 2017. Removing bias from LiDAR-based estimates of canopy height: Accounting for the effects of pulse density and footprint size. Remote Sensing of Environment 198, 1–16. URL: https://linkinghub.elsevier.com/retrieve/pii/S0034425717302316, doi:10.1016/j.rse.2017.05.032.

Schneider, F., Kükenbrink, D., Schaepman, M., Schimel, D., Morsdorf, F., 2019a. Quantifying 3D structure and occlusion in dense tropical and temperate forests using close-range LiDAR. Agricultural and Forest Meteorology 268. doi:10.1016/j.agrformet.2019.01.033.

Schneider, F.D., Kükenbrink, D., Schaepman, M.E., Schimel, D.S., Morsdorf,

F., 2019b. Quantifying 3D structure and occlusion in dense tropical and temperate forests using close-range LiDAR. Agricultural and Forest Meteorology 268, 249–257. URL: https://linkinghub.elsevier.com/retrieve/pii/S0168192319300267, doi:10.1016/j.agrformet.2019.01.033.

Schneider, F.D., Leiterer, R., Morsdorf, F., Gastellu-Etchegorry, J.P., Lauret, N., Pfeifer, N., Schaepman, M.E., 2014. Simulating imaging spectrometer data: 3D forest modeling based on LiDAR and in situ data. Remote Sensing of Environment 152, 235–250. doi:10.1016/j.rse.2014.06.015.

Seidel, D., Fleck, S., Leuschner, C., Hammett, T., 2011. Review of ground-based methods to measure the distribution of biomass in forest canopies. Annals of Forest Science 68, 225–244. doi:10.1007/s13595-011-0040-z.

Sofia, S., Giannetti, F., Buscarini, S., Chirici, G., Corezzola, S., Maetzke, F.G., Miozzo, M., Travaglini, D., Veca, D.S.L.M., 2024. Comparing efficiency, timing and costs of different walking paths in HMLS LIDAR survey. Annals of Forest Research 67, 87–107. doi:10.15287/afr.2024.3671.

Soma, M., Pimont, F., Allard, D., Fournier, R., Dupuy, J.L., 2020. Mitigating occlusion effects in Leaf Area Density estimates from Terrestrial LiDAR through a specific kriging method. Remote Sensing of Environment 245, 111836. doi:10.1016/j.rse.2020.111836.

Soma, M., Pimont, F., Dupuy, J.L., 2021. Sensitivity of voxel-based estimations of leaf area density with terrestrial LiDAR to vegetation structure

and sampling limitations: A simulation experiment. Remote Sensing of Environment 257, 112354. doi:10.1016/j.rse.2021.112354.

Soma, M., Pimont, F., Durrieu, S., Dupuy, J.L., 2018. Enhanced Measurements of Leaf Area Density with T-LiDAR: Evaluating and Calibrating the Effects of Vegetation Heterogeneity and Scanner Properties. Remote Sensing 10, 1580. doi:10.3390/rs10101580.

Terryn, L., Calders, K., Bartholomeus, H., Bartolo, R.E., Brede, B., D'hont, B., Disney, M., Herold, M., Lau, A., Shenkin, A., Whiteside, T.G., Wilkes, P., Verbeeck, H., 2022. Quantifying tropical forest structure through terrestrial and UAV laser scanning fusion in Australian rainforests. Remote Sensing of Environment 271, 112912. doi:10.1016/j.rse.2022.112912.

Toivonen, J., Kangas, A., Maltamo, M., Kukkonen, M., Packalen, P., 2023. Assessing biodiversity using forest structure indicators based on airborne laser scanning data. Forest Ecology and Management 546, 121376. doi:10.1016/j.foreco.2023.121376.

Torralba, J., Carbonell-Rivera, J.P., Ruiz, L.Á., Crespo-Peremarch, P., 2022. Analyzing TLS Scan Distribution and Point Density for the Estimation of Forest Stand Structural Parameters. Forests 13, 2115. doi:10.3390/f13122115.

van der Tol, C., Verhoef, W., Timmermans, J., Verhoef, A., Su, Z., 2009. An integrated model of soil-canopy spectral radiances, photosynthesis, flu-

orescence, temperature and energy balance. Biogeosciences 6, 3109–3129. doi:10.5194/bg-6-3109-2009.

Vincent, G., Antin, C., Laurans, M., Heurtebize, J., Durrieu, S., Lavalley, C., Dauzat, J., 2017. Mapping plant area index of tropical evergreen forest by airborne laser scanning. A cross-validation study using LAI2200 optical sensor. Remote Sensing of Environment 198, 254–266. doi:10.1016/j.rse.2017.05.034.

Wagner, W., Hollaus, M., Briese, C., Ducic, V., 2008. 3D vegetation mapping using small-footprint full-waveform airborne laser scanners. International Journal of Remote Sensing 29, 1433–1452. URL: https://www.tandfonline.com/doi/full/10.1080/01431160701736398, doi:10.1080/01431160701736398.

Wang, W., Li, Y., Huang, H., Hong, L., Du, S., Xie, L., Li, X., Guo, R., Tang, S., 2023. Branching the limits: Robust 3d tree reconstruction from incomplete laser point clouds. International Journal of Applied Earth Observation and Geoinformation 125, 103557. doi:10.1016/J.JAG.2023.103557. publisher: Elsevier.

Wang, Y., Fang, H., 2020. Estimation of LAI with the LiDAR technology: A review. Remote Sensing 12, 3457. URL: https://www.mdpi.com/2072-4292/12/20/3457, doi:10.3390/rs12203457.

Wei, S., Yin, T., Dissegna, M.A., Whittle, A.J., Ow, G.L.F., Yusof, M.L.M.,

Lauret, N., Gastellu-Etchegorry, J.P., 2020. An assessment study of three indirect methods for estimating leaf area density and leaf area index of individual trees. Agricultural and Forest Meteorology 292-293, 108101. URL: https://www.sciencedirect.com/science/article/pii/S0168192320302033, doi:https://doi.org/10.1016/j.agrformet.2020.108101.

Widlowski, J.L., Mio, C., Disney, M., Adams, J., Andredakis, I., Atzberger, C., Brennan, J., Busetto, L., Chelle, M., Ceccherini, G., Colombo, R., Côté, J.F., Eenmäe, A., Essery, R., Gastellu-Etchegorry, J.P., Gobron, N., Grau, E., Haverd, V., Homolová, L., Huang, H., Hunt, L., Kobayashi, H., Koetz, B., Kuusk, A., Kuusk, J., Lang, M., Lewis, P.E., Lovell, J.L., Malenovský, Z., Meroni, M., Morsdorf, F., Mõttus, M., Ni-Meister, W., Pinty, B., Rautiainen, M., Schlerf, M., Somers, B., Stuckens, J., Verstraete, M.M., Yang, W., Zhao, F., Zenone, T., 2015. The fourth phase of the radiative transfer model intercomparison (RAMI) exercise: Actual canopy scenarios and conformity testing. Remote Sensing of Environment 169, 418–437. doi:10.1016/j.rse.2015.08.016.

Wilkes, P., Lau, A., Disney, M., Calders, K., Burt, A., Gonzalez de Tanago, J., Bartholomeus, H., Brede, B., Herold, M., 2017. Data acquisition considerations for Terrestrial Laser Scanning of forest plots. Remote Sensing of Environment 196, 140–153. doi:10.1016/j.rse.2017.04.030.

Williams, A., Barrus, S., Morley, R.K., Shirley, P., 2005. An efficient and

robust ray-box intersection algorithm, in: ACM SIGGRAPH 2005 Courses on - SIGGRAPH '05, ACM Press, Los Angeles, California. p. 9. URL: http://portal.acm.org/citation.cfm?doid=1198555.1198748, doi:10.1145/1198555.1198748.

Winiwarter, L., Esmorís Pena, A.M., Weiser, H., Anders, K., Martínez Sánchez, J., Searle, M., Höfle, B., 2022. Virtual laser scanning with helios++: A novel take on ray tracing-based simulation of topographic full-waveform 3d laser scanning. Remote Sensing of Environment 269, 112772. URL: https://www.sciencedirect.com/science/article/pii/S0034425721004922, doi:https://doi.org/10.1016/j.rse.2021.112772.

Xu, H., Huai, Y., Zhao, X., Meng, Q., Nie, X., Li, B., Lu, H., 2025. SK-TreePCN: Skeleton-embedded transformer model for point cloud completion of individual trees from simulated to real data. Remote Sensing 17, 656. URL: https://www.mdpi.com/2072-4292/17/4/656, doi:10.3390/rs17040656. number: 4 Publisher: Multidisciplinary Digital Publishing Institute.

Yin, D., Wang, L., Lu, Y., Shi, C., 2024. Mangrove tree height growth monitoring from multi-temporal uav-lidar. Remote Sensing of Environment 303, 114002. URL: https://www.sciencedirect.com/science/article/pii/S0034425724000130, doi:https://doi.org/10.1016/j.rse.2024.114002.

Yrttimaa, T., Saarinen, N., Kankare, V., Viljanen, N., Hynynen, J., Hu-

uskonen, S., Holopainen, M., Hyyppä, J., Honkavaara, E., Vastaranta, M., 2020. Multisensorial Close-Range Sensing Generates Benefits for Characterization of Managed Scots Pine (Pinus sylvestris L.) Stands. ISPRS International Journal of Geo-Information 9, 309. doi:10.3390/ijgi9050309.

Yun, T., Cao, L., An, F., Chen, B., Xue, L., Li, W., Pincebourde, S., Smith, M.J., Eichhorn, M.P., 2019. Simulation of multi-platform LiDAR for assessing total leaf area in tree crowns. Agricultural and Forest Meteorology 276-277, 107610. URL: https://linkinghub.elsevier.com/retrieve/pii/S0168192319302187, doi:10.1016/j.agrformet.2019.06.009.

Zellweger, F., De Frenne, P., Lenoir, J., Vangansbeke, P., Verheyen, K., Bernhardt-Römermann, M., Baeten, L., Hédl, R., Berki, I., Brunet, J., Van Calster, H., Chudomelová, M., Decocq, G., Dirnböck, T., Durak, T., Heinken, T., Jaroszewicz, B., Kopecký, M., Máliš, F., Macek, M., Marek, M., Naaf, T., Nagel, T.A., Ortmann-Ajkai, A., Petřík, P., Pielech, R., Reczyńska, K., Schmidt, W., Standovár, T., Świerkosz, K., Teleki, B., Vild, O., Wulf, M., Coomes, D., 2020. Forest microclimate dynamics drive plant responses to warming. Science in press, 772–775.

Zhang, T., Hu, C., Han, J., Sun, H., Wang, R., Jing, Z., 2025. TreegrowNet: a completion network for incomplete single tree point cloud from TLS. International Journal of Remote Sensing 46. URL: https://doi.org/10.1080/01431161.2024.2440134, doi:10.108

0/01431161.2024.2440134. publisher: Taylor & Francis _eprint: https://doi.org/10.1080/01431161.2024.2440134.

Zhu, Y., Li, D., Fan, J., Zhang, H., Eichhorn, M.P., Wang, X., Yun, T., 2023. A reinterpretation of the gap fraction of tree crowns from the perspectives of computer graphics and porous media theory. Frontiers in Plant Science Volume 14 - 2023. URL: https://www.frontiersin.org/journals/plant-science/articles/10.3389/fpls.2023.1109443, doi:10.3389/fpls.2023.1109443.

Appendix A. Practical guidelines for acquisition design and occlusion reporting

This appendix provides the detailed, platform- and forest-type-specific acquisition guidelines summarised in Section 3.4. Table A.5 also states reporting conventions that make occlusion-related uncertainty interpretable and reproducible. These guidelines are based on the experience and expertise of the authors, substantiated by relevant literature where applicable. We stress that the forest tzpes considered here represent a broad classification only: significant within-type variation in 3D structure, layering and density will often call for adaptive changes to the acquisition strategy, so the guidelines should be read as informed starting points rather than prescriptions guaranteeing complete coverage with minimal occlusion.

To make occlusion-related uncertainty interpretable and reproducible, occlusion should be routinely quantified and reported alongside any derived

structural metrics. At a minimum, the fraction of occluded voxels should be reported per canopy height stratum (e.g. in 2 m bins), since occlusion effects are strongly height-dependent and differ systematically between above- and below-canopy platforms. For metrics known to be particularly sensitive to occlusion, such as LAI/PAI, PAD, quantitative structure models (QSM), and box dimension (Table 4, the occluded volume fraction should be treated as a formal quality flag, and results from acquisitions exceeding a study-specific threshold should either be excluded or corrected prior to analysis (Schneider et al., 2019b; Béland et al., 2014; Nguyen et al., 2022).

Finally, the metadata stored alongside any point cloud should include scan position or trajectory information, the voxel siye used for occlusion mapping, and the software tool applied, since these parameters directly affect the quantified occlusion fraction and are essential for any future reanalysis or cross-dataset comparison (as further discussed in Section 3.5.

Table A.5: Practical guidelines for laser scanning acquisition design by forest type and platform. These guidelines are based on experience and expertise by the authors, with supporting literature cited where applicable. *Occlusion hotspot* denotes the canopy zone most susceptible to occlusion for the given platform–forest type combination. All recommendations assume comprehensive 3D structural characterisation as the primary goal. Further, examples for metrics requiring special attention are mentioned explicitly (e.g. QSM, LAI/PAI).

Forest type	**Platform**	**Acquisition design**	**Occlusion hotspot**	**Mitigation priority**	**Reporting recommendation**
Boreal / temperate coniferous	ALS / ULS	ALS: ⩾50 % lateral strip overlap (Kükenbrink et al., 2017); ULS: orthogonal double-grid + 45° diagonal (Brede et al., 2022; Morsdorf et al., 2025); maximum sensor FOV; lower flight altitude preferred for ULS (Gassilloud et al., 2025).	Understory, especially for dense young conifer patches; Within dense crowns.	Add cross-grid flight lines (Brede et al., 2022; Gassilloud et al., 2025); complement with ground-based scanning (TLS or MLS) if sub-crown metrics (e.g. LAI/PAD) are required (Schneider et al., 2019a);	Report occluded voxel fraction per height stratum (e.g. 2 m bins); flag LAI/PAD estimates with voxel-level sampling adequacy.
(cont.)	TLS	Regular grid, 10-20 m between stations (depending on stand density) (Wilkes et al., 2017); multi-return sensor preferred (Calders et al., 2014); denser placement close to or in very dense patches.	Upper crowns; behind trunks at single-station positions.	Increase station density in denser areas (Abegg et al., 2017); use iterative placement optimisation when prior structural information is available (Li et al., 2020).	Report per-station and merged occlusion maps; record station spacing and count in metadata; flag QSM-derived metrics where occluded fraction exceeds a defined threshold.

Continued on next page

Table A.5 – continued from previous page

Forest type	Platform	Acquisition design	Occlusion hotspot	Mitigation priority	Reporting recommendation
Temperate broadleaf (leaf-on)	ULS / ALS	ALS: ⩾50 % lateral strip overlap (Kükenbrink et al., 2017); ULS: Orthogonal double-grid + 45° diagonal (Brede et al., 2022; Morsdorf et al., 2025); maximum scan angle; low flight altitude (e.g. 10-20 m above canopy) to maximise pulse density (Gassilloud et al., 2025); complement with MLS or TLS for lower canopy.	Lower third of canopy; understory; dense foliage creates a sharp occlusion boundary.	ULS + MLS/TLS fusion strongly recommended (Schneider et al., 2019a; Terryn et al., 2022); leaf-off complementary acquisition for sub-canopy structural targets (Davison et al., 2020).	Report stratum-wise occlusion; compare leaf-on and leaf-off occluded volume fractions to isolate the phenological effect; report PAD sampling adequacy per voxel; record phenological state (DOY) and wind conditions in metadata.
(cont.)	TLS / MLS	TLS: ⩽10 m grid spacing (Wilkes et al., 2017); multi-return system preferred (Calders et al., 2014). MLS: star-shaped or double-grid pattern (Sofia et al., 2024; Mokroš et al., 2021); avoid single-loop designs.	Upper canopy (both); MLS more severely affected than TLS due to larger beam footprint and often only single-return capabilities; dense understory exacerbates effect.	Complement with ULS for canopy-top metrics (Schneider et al., 2019a); use multi-return TLS where available (Abegg et al., 2021; Calders et al., 2014); increase scanning density (closer scan stations / trajectory spacing).	Stratify occlusion by height; flag tree-height estimates from ground-based systems where upper-canopy occlusion exceeds a defined threshold (Mathes et al., 2023); record phenological state, wind condition and sensor type.

Continued on next page

Table A.5 – continued from previous page

Forest type	Platform	Acquisition design	Occlusion hotspot	Mitigation priority	Reporting recommendation
Temperate broadleaf (leaf-off)	ULS / ALS	ALS: ⩾50 % lateral strip overlap (Kükenbrink et al., 2017); ULS: orthogonal double-grid + 45° diagonal (Brede et al., 2022; Morsdorf et al., 2025; Gassilloud et al., 2025); standard altitude acceptable as leaf-off penetration is good; leaf-off timing is itself the primary occlusion mitigation for above-canopy platforms.	Generally low; residual occlusion in lower canopy / understory of dense conifer admixtures in mixed stands.	Schedule acquisition during leaf-off where sub-canopy or terrain targets matter (Davison et al., 2020); add cross-grid lines for residual lower-canopy gaps; ground-based complement rarely needed for CHM/terrain.	Record phenological state (leaf-off, DOY) and wind conditions in metadata; report occluded voxel fraction per height stratum; where multi-temporal, compare against leaf-on occluded fraction to isolate the phenological effect (Davison et al., 2020).
(cont.)	TLS / MLS	TLS: Standard grid acceptable (⩽10–20 m); MLS: simpler loop or grid adequate; optimal conditions for stem, branch, and QSM targets.	Minimal; residual occlusion at upper crown (esp. for conifers) and in dense young conifer patches for mixed stands.	Low-occlusion scenario and therefore desired condition for many structural parameters;	Record phenological state (leaf-off) and wind conditions in metadata; apply lower acceptable occlusion thresholds for quality flagging; QSM and DBH estimates are most reliable under these conditions (Davison et al., 2020).

Continued on next page

Table A.5 – continued from previous page

Forest type	Platform	Acquisition design	Occlusion hotspot	Mitigation priority	Reporting recommendation
Tropical evergreen	TLS + ULS fusion	Dense TLS grid (5–10 m) (Wilkes et al., 2017); ULS: orthogonal double-grid + diagonal at maximum overlap and scan angle (10-20 m flight line distance); platform fusion is the recommended baseline (Schneider et al., 2019a; Terryn et al., 2022).	Pervasive at all canopy levels; most severe occlusion of any forest type for any single platform.	Above + below canopy combination essentially mandatory to reach maximum canopy observation (Schneider et al., 2019a); narrow beam-divergence, multi-return sensors preferred (Abegg et al., 2021; Calders et al., 2014); intermediate-height scanning (poles, scaffolds, canopy cranes) further reduces crown occlusion (D'hont et al., 2025).	Always quantify and report occlusion; LAI/PAD estimates require explicit bias correction for occluded voxels (Schneider et al., 2019a); report occluded fraction per stratum and in total.
(cont.)	ALS / ULS only	Maximum overlap and scan angle; crossed grids mandatory (Brede et al., 2022; Gassilloud et al., 2025); lowest feasible flight altitude within operational constraints.	Sub-canopy and understory effectively inaccessible to a single above-canopy platform.	Restrict analysis to canopy-surface metrics (CHM, cover fraction) unless complementary ground-based data are available; explicitly acknowledge sub-canopy limitation.	Report canopy penetration depth as a function of occluded fraction by height stratum; explicitly state that sub-canopy structural metrics are unreliable.

Continued on next page

Table A.5 – continued from previous page

Forest type	Platform	Acquisition design	Occlusion hotspot	Mitigation priority	Reporting recommendation
Plantation (any species)	ALS / ULS TLS / MLS	Exploit known row geometry: regular structure permits sparser station grids than natural forests.	Behind trunks along the planting-row direction (geometric, predictable, row-aligned).	Prior knowledge of row spacing and orientation highly beneficial; iterative scan placement optimisation (Li et al., 2020) particularly effective; occlusion severity substantially lower than natural forests.	Occlusion reporting standards as for natural forests still apply; record row geometry and its orientation relative to the acquisition direction in metadata.